Table 1
List of genes showing at least a 1.5 fold difference with $p < 0.01$ (uncorrected t-test) between methylcellulose and corn oil at any point during 24 h after single dose or at 29th day of repeated dose

Probe set ID	Gene title	Gene symbol	3 h	6 h	9 h	24 h	29 d
1367707_at	fatty acid synthase	Fasn	0.995	1.738	1.300	0.722	0.596
1367708_a_at	fatty acid synthase	Fasn	0.982	1.500	1.182	0.826	0.678
1367729_at	ornithine aminotransferase	Oat	1.223	1.140	1.066	0.792	0.653
1367836_at	carnitine palmitoyltransferase 1, liver	Cpt1a	1.325	1.483	1.535	0.888	1.305
1367854_at	ATP citrate lyase	Acly	1.081	1.741	1.295	0.882	0.760
1367946_at	PDZ and LIM domain 1 (elfin)	Pdlim1	0.762	0.661	0.777	0.914	0.977
1367959_a_at	sodium channel, voltage-gated, type I, beta polypeptide	Scn1b	1.042	1.013	1.567	1.613	1.278
1368035_a_at	protein tyrosine phosphatase, receptor type, F	Ptprf	0.935	1.009	0.649	0.920	0.985
1368160_at	insulin-like growth factor binding protein 1	Igfbp1	1.239	0.485	1.238	0.631	1.143
1368272_at	glutamate oxaloacetate transaminase 1	Got1	1.623	0.989	0.965	0.687	0.813
1368275_at	sterol-C4-methyl oxidase-like	Sc4mol	0.902	1.224	1.552	0.929	0.857
1368428_at	X-prolyl aminopeptidase (aminopeptidase P) 2, membrane-bound	Xpnpep2	0.839	0.896	0.668	0.783	0.916
1368435_at	cytochrome P450, family 8, subfamily b, polypeptide 1	Cyp8b1	1.534	1.860	1.570	0.711	0.798
1368458_at	cytochrome P450, family 7, subfamily a, polypeptide 1	Cyp7a1,	0.471	1.768	1.310	0.586	0.607
1368569_at	aldo-keto reductase family 1, member B7	Akr1b7	0.197	0.971	0.190	2.782	5.398
1369073_at	nuclear receptor subfamily 1, group H, member	Nr1h4	1.165	1.594	1.190	0.903	1.047
1369195_at	fatty acid binding protein 2, intestinal	Fabp2	0.901	1.135	1.022	1.753	1.753
1369238_at	inhibin beta E	Inhbe	1.441	1.553	1.067	1.034	0.934
1369415_at	basic helix-loop-helix domain containing, class B2	Bhlhb2	1.019	1.814	1.449	0.983	0.862
1369440_at	ATP-binding cassette, sub-family G (WHITE), member 8	Abcg8	0.676	0.538	0.701	0.893	1.440
1369493_at	prolactin receptor	Prlr	0.609	0.958	0.717	1.147	1.975
1369663_at	epoxide hydrolase 2, cytoplasmic	Ephx2	1.073	1.346	1.616	1.196	1.844
1369674_at	purinergic receptor P2X, ligand-gated ion channel, 5	P2rx5	1.930	0.838	0.893	0.811	1.065
1369790_at	tyrosine aminotransferase	Tat	0.771	0.624	1.094	0.735	0.837
1369864_a_at	serine dehydratase	Sds	1.509	0.429	0.872	0.482	0.538
1370024_at	Fatty acid binding protein 7, brain	Fabp7	1.044	0.964	1.057	1.312	1.524
1370336_at	pregnancy-induced growth inhibitor	Oki38	0.615	0.694	0.735	1.091	1.139
1370355_at	stearoyl-Coenzyme A desaturase 1	Scd1	1.206	1.197	1.065	0.904	0.604
1370427_at	platelet derived growth factor, alpha	Pdgfa	1.066	0.912	1.155	0.559	1.097
1371127_at	bone morphogenetic protein 1 (procollagen C-proetinase)	RGD:620739	0.815	1.175	0.950	0.991	1.557
1371234_at	fibrinogen, B beta polypeptide	Fgb	1.165	0.990	0.896	0.894	0.639
1371279_at	histone 2a /// similar to Histone H2A.1	RGD:621437	1.093	0.910	0.798	0.604	0.843
1371595_at	Transcribed locus, weakly similar to XP346694.1 Rattus norvegicus LOC360381 gene	---	0.738	0.639	0.607	0.824	0.938
1371754_at	solute carrier family 25 (mitochondrial carrier, phosphate carrier), member 25	Slc25a25	0.939	0.891	1.187	0.912	0.660
1372188_at	Endothelial cell growth factor 1 (platelet-derived) (predicted)	---	1.043	1.548	1.053	1.187	1.051
1372276_at	Transcribed locus	---	0.941	1.673	1.209	1.340	1.714
1372536_at	Chaperone, ABC1 activity of bc1 complex like (S. pombe) (predicted)	---	0.953	0.973	0.659	0.904	1.082
1374265_at	Similar to arylacetamide deacetylase (esterase) (predicted)	---	0.964	1.221	1.511	0.872	0.853
1374932_at	---	---	0.818	1.705	0.745	1.055	0.897
1375367_at	PDZ and LIM domain 2	Pdlim2	1.283	1.623	1.002	0.870	0.896
1375422_at	---	---	1.094	0.936	1.875	1.039	1.025
1375552_at	---	---	0.889	1.176	0.927	0.932	1.584

Data are expressed as the ratio of gene expression (methylcellulose=1) and columns with significant change are shaded ($N=15$ for each group).

together with food consumption (C). Although both methylcellulose and corn oil groups got weight in the same rate during repeated dosing, food consumption in the corn oil group was significantly lower than that in methylcellulose group by about 15% throughout the period of repeated administration.

Among the hematological and blood biochemical parameters, mean corpuscular hemoglobin concentration (at 15th day), platelets (at 9 h), monocytes (at 3 h), prothrombin time (at 29th day), activated partial thromboplastin time (at 24 h), fibrinogen (at 3 h), chloride (at 3 h) showed statistically significant differences between corn oil and methylcellurose. However, these changes were not considered to be important, since their changes were small and no changes in related parameters were associated. On the other hand, total cholesterol, phospholipids, triglyceride, and bilirubin (both total and direct) were found to be significantly different between vehicle controls (Fig. 2A–E). All of them showed significantly higher values in the corn oil group at 3 h after dosing, and the differences abated or disappeared at 6 h or later. In the repeated administration, the corn oil group showed rather lower values of triglyceride, total and direct bilirubin. Inorganic phosphate showed a significantly higher value in corn oil at 9 h and went down to a lower value than methylcellulose (Fig. 2F). Blood urea nitrogen (Fig. 2G) showed a lower value in corn oil at 6 h and 15th day.

Scatter plots of gene expression between vehicle controls at each time point revealed that most of the genes distributed within a 2-fold range of their 45° line, meaning that few

Table 1 (*continued*)

Probe set ID	Gene title	Gene symbol	3 h	6 h	9 h	24 h	29 d
1375619_at	---	---	1.171	0.667	0.789	0.971	0.756
1375796_at	interferon gamma induced GTPase (predicted)	Igtp_predicted	1.005	0.883	1.021	1.787	0.847
1376313_at	two pore segment channel 2 (predicted)	RGD:1311779	1.040	0.800	0.871	0.991	1.956
1376657_at	immunoglobulin superfamily, member 4A (predicted)	Igsf4a_predicted	1.060	1.749	1.510	0.868	1.022
1376704_a_at	necdin-like 2 (predicted)	Ndnl2_predicted	1.048	0.886	1.061	0.995	0.660
1376892_at	---	---	1.109	0.949	0.854	0.654	0.953
1376958_at	Similar to serine (or cysteine) proteinase inhibitor, clade B, member 9	---	0.456	0.824	1.105	1.206	1.039
1377361_at	---	---	1.004	0.667	0.794	0.890	1.020
1379252_at	Immunoglobulin superfamily, member 4A (predicted)	---	1.083	1.505	1.476	0.861	0.970
1383075_at	cyclin D1	Ccnd1	0.636	0.693	0.945	1.029	1.211
1384178_at	Leucine rich repeat containing 4B (predicted)	---	0.906	0.656	0.890	0.802	0.884
1384288_at	Transcribed locus	---	1.119	0.596	1.136	0.835	1.054
1386041_a_at	Kruppel-like factor	Klf2	1.986	0.850	1.345	1.004	1.053
1386789_at	---	---	1.305	0.611	1.196	1.134	1.003
1387017_at	squalene epoxidase	Sqle	0.927	1.279	1.852	1.058	0.980
1387022_at	aldehyde dehydrogenase family 1, member A1	Aldh1a1	0.769	1.099	0.913	1.039	1.804
1387123_at	cytochrome P450, family 17, subfamily a, polypeptide 1	Cyp17a1	1.003	0.982	1.106	1.309	1.613
1387183_at	carnitine O-octanoyltransferase	Crot	1.058	1.116	1.142	0.914	1.569
1387283_at	myxovirus (influenza virus) resistance 2	Mx2	0.721	0.777	0.503	1.565	1.280
1387307_at	histidine ammonia lyase	Hal	0.903	0.826	0.665	0.819	1.072
1387312_a_at	glucokinase	Gck	1.180	1.610	0.865	0.941	1.077
1387391_at	cyclin-dependent kinase inhibitor 1A	Cdkn1a	1.576	1.373	0.734	0.684	0.892
1387396_at	hepcidin antimicrobial peptide	Hamp	0.731	0.642	1.232	1.145	1.051
1387643_at	fibroblast growth factor 21	Fgf21	1.385	1.919	1.138	1.191	1.157
1387665_at	betaine-homocysteine methyltransferase	Bhmt	1.234	1.064	1.083	0.655	0.850
1387670_at	glycerol-3-phosphate dehydrogenase 2	Gpd2	1.169	1.650	1.430	0.872	0.864
1387730_at	paired box gene 8	Pax8	1.527	1.114	0.991	0.822	0.827
1387809_at	mitogen-activated protein kinase kinase 6	Map2k6	1.017	1.443	1.139	0.622	0.742
1387848_at	3-hydroxy-3-methylglutaryl-Coenzyme A reductase	Hmgcr	0.810	1.306	1.962	1.057	0.876
1388210_at	mitochondrial acyl-CoA thioesterase 1	Mte1	1.085	1.245	1.928	1.099	1.120
1388395_at	G0/G1 switch gene 2 (predicted)	G0s2_predicted	2.129	1.930	1.041	1.204	1.036
1388426_at	sterol regulatory element binding factor 1	Srebf1	0.648	0.787	0.694	0.855	0.885
1388531_at	progesterone receptor membrane component 2 (predicted)	Pgrmc2 predicted	1.032	1.518	1.149	0.938	1.036
1388679_at	TBC1 domain family, member 14 (predicted)	Tbc1d14 predicted	0.815	1.582	1.111	0.883	1.038
1388792_at	growth arrest and DNA-damage-inducible 45 gamma (predicted)	Gadd45 gpredicted	0.340	1.095	0.994	0.669	0.595
1388872_at	Isopentenyl-diphosphate delta isomerase	Idi1	1.029	1.077	1.772	1.249	0.870
1388924_at	angiopoietin-like protein 4	Angptl4	2.172	1.589	1.105	0.673	0.990
1389161_at	Transcribed locus	---	1.547	1.566	1.153	0.819	1.014
1389253_at	vanin 1 (predicted)	Vnn1 predicted	1.127	1.614	1.846	1.232	1.650
1389430_at	Transcribed locus	---	0.917	1.198	1.517	0.863	1.008
1390383_at	adipose differentiation-related protein	ADRP	1.296	1.784	0.870	0.952	0.913
1390607_at	nNOS-intereacting DHHC-containing Dem protein-L	RGD:1303254	0.936	1.463	1.509	0.691	0.878
1390662_at	Ab2-427	---	0.594	0.996	0.819	1.114	0.980
1392607_at	Transcribed locus	---	0.756	0.855	0.725	0.441	1.298

genes were affected by the vehicle (data not shown). Table 1 shows the list of genes that showed at least a 1.5-fold difference between vehicles with $p<0.01$ either in single dose experiment or in the 29th day of repeated dosing. Many of the genes listed are related to lipid metabolism. They were usually up-regulated by corn oil between 3 and 9 h after dosing and returned to the same level or lower at 24 h and at the 29th day. However, there were some exceptional cases, such as aldo-keto reductase 1B7 (down-regulated at 3 and 9 h but up-regulated at 24 h and 29th day), or aldehyde dehydrogenase 1A1 (only up-regulated after repeated administration). Among the genes in Table 1, there are interesting ones, i.e., CYP7A1, CYP8B1, 3-hydroxy-3-methylglutaryl-Coenzyme A reductase, fatty acid synthase, squalene epoxidase, angiopoietin-like protein 4, which are selected and shown as graphs in Fig. 3A–F. The former 5 genes all showed a circadian rhythm in that their expression in the afternoon to the evening was higher than that in the morning to noon. The administration of corn oil appeared to increase this peak. On the other hand, angiopoietin-like protein 4 showed constant expression during the day in methylcellulose, whereas corn oil markedly increased the expression of this gene at 3 and 6 h of administration.

As is obvious from Figs. 1A and 3, there exists a circadian rhythm in rat liver. In order to examine whether the observed changes were due to a disturbance in the basic rhythm, expression of various clock genes were checked and we found that the rhythm (other than that related to lipid metabolism) was relatively unaffected. As typically representative of clock genes, the expression patterns of period 2, D site albumin

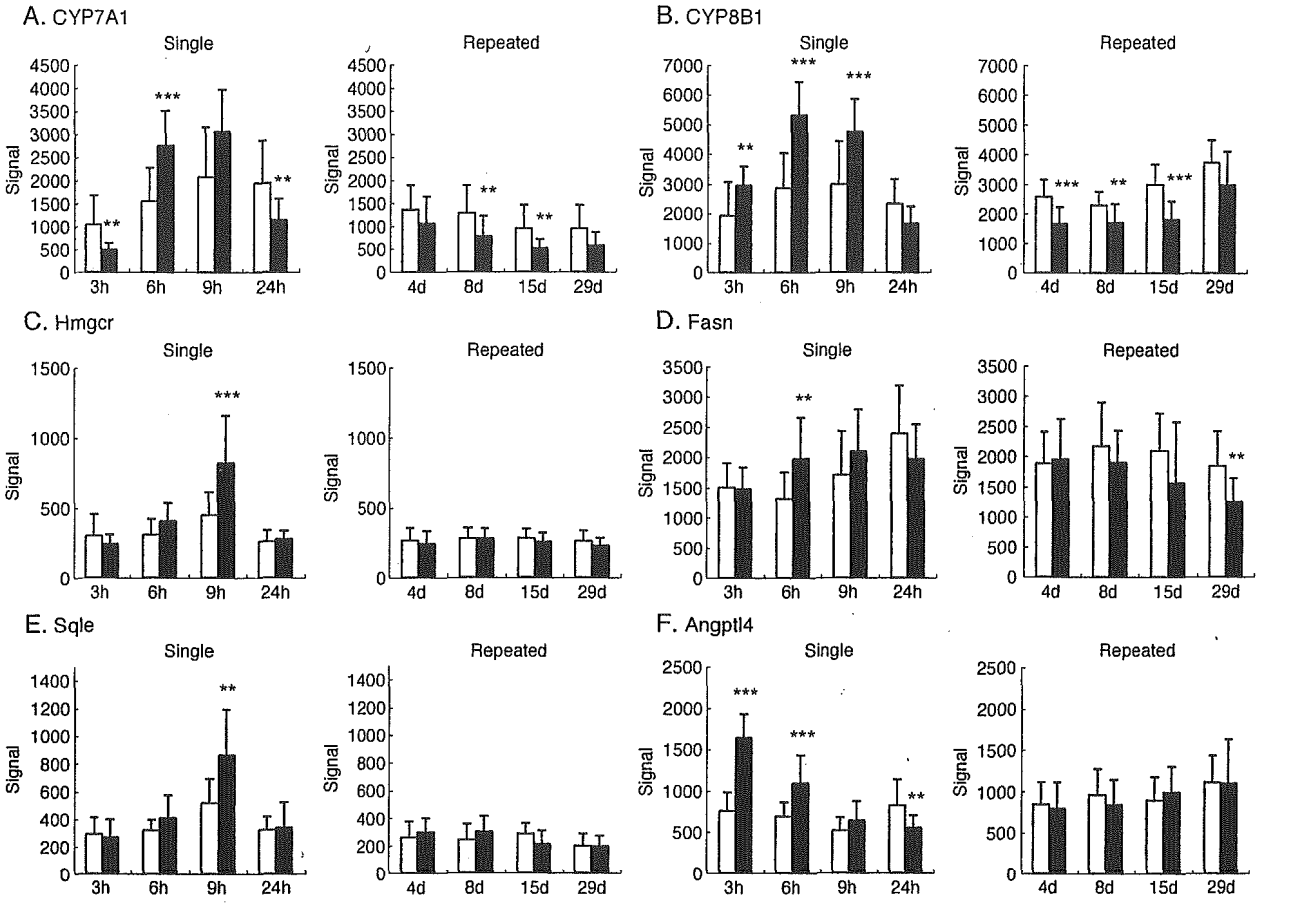

Fig. 3. Expression changes of CYP7A1 (A, Affymetrix ID 1368458_at), CYP8B1(B, Affymetrix ID 368435_at), 3-hydroxy-3-methylglutaryl-Coenzyme A reductase (C, Affymetrix ID 1387848_at), fatty acid synthase (D, Affymetrix ID 1367708_a_at), squalene opixidase (E, Affymetrix ID 1387017_at) and angiopoietin-like protein 4 (F, Affymetrix ID 1388924_at) are shown. Open and filled symbols represent methylcellulose and corn oil, respectively. Values are expressed as mean±SD of 15 rats of each for each time point. Statistically significant between methylcellulose and corn oil by uncorrected Student's *t*-test at $^{**}p<0.01$, $^{***}p<0.001$.

promoter binding protein, and arylhydrocarbon receptor nuclear translocator-like are shown in Fig. 4A–C.

Discussion

The ultimate goal of our project is to create a gene expression database for prediction of hepatotoxicity in the early stage of drug development. For this purpose, it was desirable that the vehicle for suspending drugs was unified to be methylcellulose. However, there are many test compounds with poor dispersibility, and strong detergents or organic solvents are undesirable because of their potent bioactivity, so we inevitably chose corn oil as a vehicle for the highly hydrophobic compounds.

Corn oil contains 9.2 kcal/g and supplies 10.1 kcal/day for 7-week-old rats (5 ml/kg corresponds to 1.1 g for 250 g body weight). Rats around this age consume about 25 g diet per day in the present study (Fig. 1C), which corresponds to about 90 kcal/day (CRF-1 carries 3.6 kcal/g), meaning that the administered corn oil is equal to about 11% of the total calories. Moreover, this is administered once in the morning when the feeding behavior of the rat is normally inactive. Then we were concerned that the difference between corn oil and methylcellulose cannot be ignored. In fact, the food intake of the rats in the corn oil group was significantly decreased by about 15% compared with methylcellulose group without any changes in body weight. This suggests that the rats self-controlled their total calorie intake to a constant level and so corresponding gene expression changes should have occurred.

In the acute phase, total cholesterol, triglyceride, phospholipids, and bilirubin were elevated 3 h after the administration of corn oil, which were considered to be due to rapid absorption of oil. We are not sure why plasma bilirubin was increased; it might reflect an increase in the absorption of bile components when large amounts of lipid were absorbed in the form of micelle. These parameters all returned to the same level as in the methylcellulose group 6–9 h after administration. In the repeated dose experiments, which correspond to 24 h after dosing, triglyceride and bilirubin were decreased in the corn oil group, suggesting that some adapting system lowering plasma lipid was induced during a continuous elevation of lipid component in the diet.

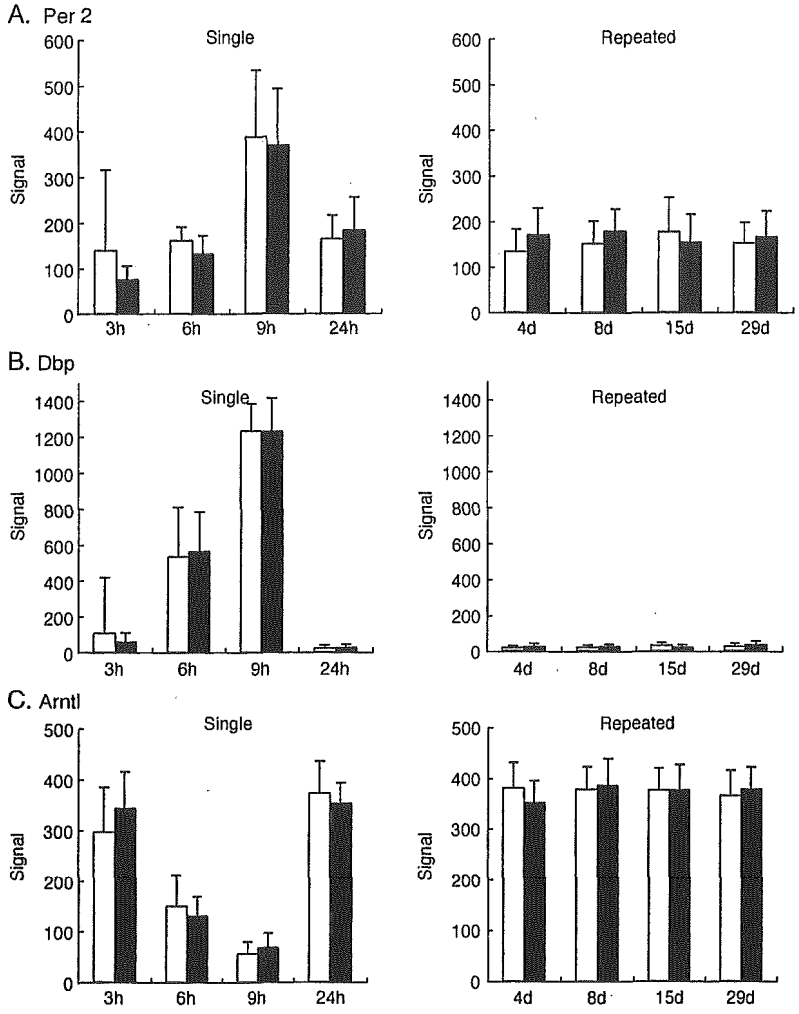

Fig. 4. Expression patterns of representative clock genes, period 2 (A, Affymetrix ID 1368303_at), D site albumin promoter binding protein (B, Affymetrix ID 1387874_at), and arylhydrocarbon receptor nuclear translocator-like (C, Affymetrix ID 1370510_a_at) are shown. Open and filled symbols represent methylcellulose and corn oil, respectively. Values are expressed as mean±SD of 15 rats for each time point. No statistically significant difference was observed between methylcellulose and corn oil at any time point.

The change in gene expression in the liver was more complex. Although the numbers of differentially expressed genes were small in respect of the total 16,000 probe sets, there were still considerable numbers of genes showing different patterns between vehicles, most of which were related to lipid metabolism. In the corn oil-treated group, the expression of CYP7A1 (cholesterol 7α hydroxylase), the rate-limiting enzyme of bile acid synthesis or elimination of cholesterol (Mast et al., 2005), showed a clear circadian rhythm as reported (Kai et al., 1995; Ishida et al., 2000), and it was lower at 3 h but higher at 6 and 9 h than that in the methylcellulose group. The expression was then lowered again at 24 h after dosing, and this pattern appeared to continue during repeated administration, i.e., the expression value in the corn oil group stayed about 60% of those in the methylcellulose group until the 29th day. On the other hand, CYP 8B1 (cholesterol 12α hydroxylase), which catalyzes the synthesis of cholic acid and controls the ratio of cholic acid over chenodeoxycholic acid in the bile, showed a less marked but obvious circadian pattern as reported (Ishida et al., 2000). It showed a continuously higher expression from 3 to 9 h than methylcellulose, returned to the same level at 24 h, and no difference was observed in the repeated dosing. These changes were considered to be the reflection of the transiently high consumption of bile due to the bolus injection of corn oil.

The rate-limiting enzyme of cholesterol biosynthesis, 3-hydroxy-3-methylglutaryl-Coenzyme A reductase, also showed a circadian rhythm and the administration of corn oil markedly increased its expression at 9 h. At this point, squalene epoxidase and sterol-C4-methyloxidase were also increased. The former is a microsomal enzyme that catalyzes the oxidation of squalene to 2,3-oxidosqualene, the last reaction of non-sterol metabolites in the cholesterol biosynthesis pathway (Hidaka et al., 1990). The latter is known as one of the components essential for sterol biosynthesis in yeast (Darnet and Rahier, 2003), and it used to be termed neurorep1 and was discussed in relation to the repair

process of damaged neurons (Uwabe et al., 1997). Looking at the high expression level in liver and induction by corn oil alone, we considered that the induction of sterol-C4-methyloxidase was a general phenomenon related to lipid metabolism rather than neurophysiology.

One noticeable gene is angiopoietin-like protein 4, which was recently shown to be involved not only in lipid metabolism via inhibition of lipoprotein lipase activity (Yoshida et al., 2002) but also in various diseases (Xu et al., 2005). It was reported that its expression in adipose tissue and liver was affected by the nutrient status, e.g., induced by fasting (Ge et al., 2005). In the present study, this gene was markedly up-regulated at 3–6 h after corn oil treatment and returned to the same level as methylcellulose at 9 h or later. It is of interest to elucidate why oil intake resembles fasting in case of angiopoietin-like protein 4 expression.

Fatty acid synthase was up-regulated by corn oil at 6 h after dosing and then returned to the same level as methylcellulose, whereas it was down-regulated (about 60% of methylcellulose) after repeated administration. In contrast, fatty acid binding protein family members, involved in lipid uptake, were up-regulated 24 h after single and repeated administrations of corn oil. These reactions in the repeated phase are considered to be adaptive responses suitable for lipid intake. In addition to these two enzymes, there were genes showing significantly different expression in the corn oil group at 29th day, i.e., serine dehydratase, ornithine aminotransferase, stearoyl CoA desaturase, aldehyde dehydrogenase 1A1, and epoxide hydroxylase 2. Of these, the latter two were up-regulated whereas the others were down-regulated.

The increase of aldehyde dehydrogenase and epoxide hydroxylase is considered to be favorable for the condition of high lipid diet, since both enzymes are reported to be involved in the detoxication of the metabolites associated with lipid metabolism (Choudhary et al., 2005; Newman et al., 2005). As for the down-regulated genes, the decrease of fatty acid synthase and stearoyl CoA desaturase, both are in the pathway of fatty acid synthesis, which might reflect a decrease in the need of fatty acid. Serine dehydratase and ornithine aminotransferase are known to be induced by high protein diet, glucagon, or glucocorticoid (Hunter and Harper, 1977; Bourdel et al., 1983). Based on the present data, it is difficult to conclude whether the change was due to the relative reduction of protein in the diet, or to the secondary change in endocrinological status. Moreover, it should be noted that the circadian pattern could not be obtained in the present experiments of repeated administration. Although most of the observed changes could be interpreted as an adaptation for the rapid absorption of oil from the gut in the acute phase and for the continuously elevated composition of lipid in the food in the chronic phase, it is difficult to map all the changes to various metabolic pathways, and to give reasonable explanations. Further confirmation is obviously needed, but the present study has supplied many valuable suggestions.

Many of the genes affected by corn oil treatment exhibit their own circadian rhythm generally with low expression at 3 h (around noon), increasing from 6 h (late afternoon) to 9 h (evening), and returning to low expression at 24 h (morning) of dosing. There is a long blank period between 9 and 24 h after dosing, as it was practically impossible to perform measurements after midnight in the present project. It was therefore possible that the actual peak of some genes occurred between 9 and 24 h after dosing, or midnight. We were concerned that the compulsory administration of oil in the morning disturbs not only feeding behavior but also the circadian rhythm itself. However, it was confirmed that the expression patterns of representative clock genes were unaffected, suggesting that changes in gene expression were not due to the disturbance of the original circadian rhythm. Moreover, the expression levels of clock genes in repeated dosing (corresponding to the 24 h value) were also unchanged, suggesting that disturbance of the circadian rhythm during repeated administration of oil was unlikely.

The present analysis of the data in our database would provide useful information for future experiments to elucidate the detailed mechanism of lipid metabolism. It also provides valuable information for the analysis of the activity of compounds when a comparison of chemicals dosed with different vehicles is made. Since the data accumulated in our database appeared to be of high quality and reproducibility, at least in terms of the effect of vehicles, we expect that drug actions, especially related to toxicity, may be sensitively detected using our database.

Acknowledgements

This study was supported in part by a grant from the Ministry of Health, Labour and Welfare (H14-Toxico-001).

References

Bourdel, G., Hitier, Y., Lardeux, B., Girard-Globa, A., 1983. Activity of several enzymes of amino acid catabolism in the liver of rats fed protein as a meal. Reproduction Nutrition Development 23, 875–881.

Choudhary, S., Xiao, T., Srivastava, S., Zhang, W., Chan, L.L., Vergara, L.A., Van Kuijk, F.J., Ansari, N.H., 2005. Toxicity and detoxification of lipid-derived aldehydes in cultured retinal pigmented epithelial cells. Toxicology and Applied Pharmacology 204, 122–134.

Darnet, S., Rahier, A., 2003. Enzymological properties of sterol-C4-methyl-oxidase of yeast sterol biosynthesis. Biochimica et Biophysica Acta 1633, 106–117.

Ge, H., Cha, J.Y., Gopal, H., Harp, C., Yu, X., Repa, J.J., Li, C., 2005. Differential regulation and properties of angiopoietin-like proteins 3 and 4. Journal of Lipid Research 46, 1484–1490.

Hidaka, Y., Satoh, T., Kamei, T., 1990. Regulation of squalene epoxidase in HepG2 cells. Journal of Lipid Research 31, 2087–2094.

Hunter, J.E., Harper, A.E., 1977. Induction of pyridoxal phosphate-dependent enzymes in vitamin B-6 deficient rats. Nutrition 107, 235–244.

Ishida, H., Yamashita, C., Kuruta, Y., Yoshida, Y., Noshiro, M., 2000. Insulin is a dominant suppressor of sterol 12 alpha-hydroxylase P450 (CYP8B) expression in rat liver: possible role of insulin in circadian rhythm of CYP8B. Journal of Biochemistry (Tokyo) 127, 57–64.

Kai, M.-H., Eto, T., Kondo, K., Setoguchi, Y., Higashi, S., Maeda, Y., Setoguchi, T., 1995. Synchronous circadian rhythms of mRNA levels and activities of cholesterol 7 alpha-hydroxylase in the rabbit and rat. Journal of Lipid Research 36, 367–374.

Mast, N., Graham, S.E., Andersson, U., Bjorkhem, I., Hill, C., Peterson, J., Pikuleva, I.A., 2005. Cholesterol binding to cytochrome P450 7A1, a key enzyme in bile acid biosynthesis. Biochemistry 44, 3259–3271.

Newman, J.W., Morisseau, C., Hammock, B.D., 2005. Epoxide hydrolases: their roles and interactions with lipid metabolism. Progress in Lipid Research 44, 1–51.

Urushidani, T., Nagao, T., 2005. Toxicogenomics: the Japanese initiative. In: Borlak, J. (Ed.), Handbook of Toxicogenomics—Strategies and Applications. Wiley-VCH, pp. 623–631.

Uwabe, K., Gahara, Y., Yamada, H., Miyake, T., Kitamura, T., 1997. Identification and characterization of a novel gene (neurorep 1) expressed in nerve cells and up-regulated after axotomy. Neuroscience 80, 501–509.

Waring, J.F., Ulrich, R.G., Flint, N., Morfitt, D., Kalkuhl, A., Staedtler, F., Lawton, M., Beekman, J.M., Suter, L., 2004. Interlaboratory evaluation of rat hepatic gene expression changes induced by methapyrilene. Environmental Health Perspectives 112, 439–448.

Xu, A., Lam, M.C., Chan, K.W., Wang, Y., Zhang, J., Hoo, R.L., Xu, J.Y., Chen, B., Chow, W.S., Tso, A.W., Lam, K.S., 2005. Angiopoietin-like protein 4 decreases blood glucose and improves glucose tolerance but induces hyperlipidemia and hepatic steatosis in mice. Proceedings of the National Academy of Sciences of the United States of America 102, 6086–6091.

Yoshida, K., Shimizugawa, T., Ono, M., Furukawa, H., 2002. Angiopoietin-like protein 4 is a potent hyperlipidemia-inducing factor in mice and inhibitor of lipoprotein lipase. Journal of Lipid Research 43, 1770–1772.

THE JOURNAL OF BIOLOGICAL CHEMISTRY
Vol. 278, No. 38, Issue of September 19, pp. 36470–36475, 2003
Printed in U.S.A.

Role of ADP-ribosylation Factor 6 (ARF6) in Gastric Acid Secretion*

Received for publication, May 23, 2003, and in revised form, July 10, 2003
Published, JBC Papers in Press, July 14, 2003, DOI 10.1074/jbc.M305444200

Jun Matsukawa‡, Kazuhisa Nakayama§, Taku Nagao¶, Hidenori Ichijo‡, and Tetsuro Urushidani‡¶‖

From the ‡Laboratory of Cell Signaling, Graduate School of Pharmaceutical Sciences, The University of Tokyo, Tokyo 113-0033, the §Graduate School of Pharmaceutical Sciences, Kyoto University, Kyoto 606-8501, and the ¶National Institute of Health Sciences, 1-18-1 Kamiyoga, Setagaya-ku, Tokyo 158-8501, Japan

ADP-ribosylation factor (ARF) proteins are monomeric GTPases that are essential for membrane transport and exocytosis in a number of secretory cells. We investigated ARF6, the activation of which is insensitive to brefeldin A, to determine whether it regulates membrane traffic in gastric parietal cells. ARF6 translocated from cytosol to tubulovesicle in the presence of GTPγS, a potential inhibitor of acid secretion in permeabilized cells, whereas under the Mg^{2+}-chelated condition where activity of ARF-GTPase activating protein is inhibited, ARF6 translocated to the apical secretory membrane. Immunohistochemical examination revealed that ARF6 mainly located in parietal cell within the gastric glands, and it translocated from the cytosol to the intracellular canaliculi when the glands were stimulated. These results indicated that the distribution of ARF6 between cytosol and the two different membranes was regulated by its GTPase activity. In cultured gastric glands infected with adenovirus expressing ARF6 Q67L, a mutant lacking GTP hydrolysis activity, gastric acid secretion was inhibited. These results suggest that ARF6 regulates gastric acid secretion in parietal cell and that the GTP hydrolysis cycle of ARF6 is essential for the activation pathway.

Activation of acid secretion in parietal cell involves mainly two steps: (*a*) translocation of the intracellular vesicles containing proton pump, so-called tubulovesicles or tubulocisternae, to the apical membrane, called intracellular canaliculus, and (*b*) the acquisition of potassium and chloride permeabilities, essential for operation of the pump, on the canalicular membrane. On the molecular level, this process is still unclear, but evidence has been found that suggests that regulated membrane trafficking and fusion events play the central role (1, 2). It is widely accepted that intracellular membrane traffic requires small monomeric GTPases (small G proteins), especially rab family proteins in various secretory cells (3). On the other hand, there are some observations opposing this idea. It was previously reported that GTPγS[1] strongly inhibited gastric acid secretion in α-toxin (4) or β-escin-permeabilized glands (5). These data indicate that the one or more G proteins that regulate membrane traffic in parietal cell require GTP hydrolysis for their function. Rab family proteins cannot explain the inhibitory effect of GTPγS, because they do not require GTPase activity to promote membrane transport, and non-hydrolysable GTP analogues always work as agonist (3). For these, we hypothesized that there could be one or more G proteins other than rab family that regulate membrane traffic in gastric parietal cell.

ADP-ribosylation factor (ARF) family proteins are known to regulate endocytosis, exocytosis, and membrane recycling in various secretory cells. In particular, they need their GTP-hydrolyzing activity to promote membrane transport and therefore a non-hydrolysable analogue of GTP inhibits their functions (3). We previously reported that brefeldin A, an inhibitor of ARF-guanine nucleotide exchange factor (GEF), cannot inhibit acid secretion (5). These observations interested us in ARF6, because GEF proteins for ARF6 (including ARF nucleotide-binding site opener (ARNO) and cytohesin) are known to be insensitive to this inhibitor. Although ARF1 is mainly localized to the Golgi complex and is a common regulator of non-clathrin and clathrin coat recruitment, ARF6 regulates endocytosis or exocytosis with the organization of the actin cytoskeleton, and does not co-localize with Golgi (3, 6). ARF6 is considered to be a feasible target for GTPγS, so we performed the present experiments to elucidate its possible role in regulation of membrane traffic and acid secretion in parietal cell.

EXPERIMENTAL PROCEDURES

Materials—Anti-ARF6 mouse monoclonal antibody (3A-1) was purchased from Santa Cruz Biotechnology. Anti-H^+,K^+-ATPase α-subunit rat polyclonal antibody was raised as described previously (7). The construction of an expression vector for C-terminally HA-tagged ARF6 (pcDNA3-ARF6-HA) mutant (wild type, Q67L, N122I) was described previously (8, 9). Myristoylated (myr) N-terminal peptide of ARF6 (myr-GKVLSKIFGNKE) and its reversed sequence (myr-EKNGFIKSLVKG) were custom synthesized by Qiagen. All the chemicals were reagent grade and obtained from Sigma, Nacalai Tesque, or Invitrogen except where otherwise noted.

Isolation of Gastric Glands and Preparation of Permeabilized Glands—Gastric glands were isolated from Japanese White rabbits (Shiraishi, Tokyo, Japan) essentially by the method of Berglindh (10). Isolated glands, suspended in the normal medium containing (in millimolar) 132.6 NaCl, 5 Na_2HPO_4, 1 NaH_2PO_4, 5.4 KCl, 1.2 $MgSO_4$, 1.0 $CaCl_2$, 25 HEPES-Na, pH 7.4, and 11.1 glucose with 1 mg/ml bovine serum albumin, were washed and suspended in a high K^+ medium containing (in millimolar) 20 NaCl, 100 KCl, 1.0 $MgSO_4$, 0.5 EGTA, 2 ATP, 10 sodium pyruvate, and 20 HEPES, pH 7.4. The free Ca^{2+} concentration in the high K^+ medium was calculated to be as high as 90 nM by the computer program Chelator, assuming that the contaminated Ca^{2+} in the medium was as high as 10 μM. The formation of homoge-

* This study was supported in part by the Japanese Ministry of Education, Science, Sports and Culture Grants 13470511 and 13557220. The costs of publication of this article were defrayed in part by the payment of page charges. This article must therefore be hereby marked "*advertisement*" in accordance with 18 U.S.C. Section 1734 solely to indicate this fact.

‖ To whom correspondence should be addressed. Tel.: 81-3-3700-1986; Fax: 81-3-3700-9647; E-mail: urusidani@nihs.go.jp.

[1] The abbreviations used are: GTPγS, guanosine 5′-3-*O*-(thio)triphosphate; ARF, ADP-ribosylation factor; GAP, GTPase-activating protein; GEF, guanine nucleotide exchange factor; EGFP, enhanced green fluorescent protein; myr, myristoylated; CDTA, *trans*-1,2-diaminocyclohexane-*N*,*N*,*N*′,*N*′-tetraacetic acid; PI(4,5)P_2, phosphatidylinositol 4,5-diphosphate; HA, hemagglutinin; CMV, cytomegalovirus; WT, wild type.

nous pores in the plasma membrane of gastric cells by β-escin was achieved by the modified cold incubation method as described (5). The permeabilized glands were used immediately for assay without further incubation. Acid secretion of the glands was monitored by accumulation of a weak base, [^{14}C]aminopyrine, setting water content of the glands at a constant of 2.0 ml/mg dry wt (5). The medium used for permeabilized glands was the high K^+ medium described above. To avoid the possible involvement of endogenous histamine, 100 μM cimetidine was always included, except when the glands were stimulated by histamine.

Subcellular Fractionation of the Glands—Subcellular fractionations were prepared from the homogenate as described by Urushidani and Forte (11) with a slight modification. For Mg^{2+}-dependent distribution assay, isolated glands were homogenized in the Mg^{2+}-containing buffer, containing (in millimolar) 250 sucrose, 25 HEPES, 2.5 $MgSO_4$, pH 7.4, or in the Mg^{2+}-free buffer, containing (in millimolar) 250 sucrose, 25 HEPES, 0.5 EDTA, pH 7.4. For GTPγS-dependent distribution assay, β-escin-permeabilized glands were incubated at 37 °C for 30 min in the high K^+ medium in the presence of 100 μM cimetidine or 100 μM GTPγS, and homogenized in the Mg^{2+} containing buffer. To examine the subcellular distribution of ARF6, each fraction was analyzed with SDS-PAGE according to Laemmli (12) and then blotted on a polyvinylidene difluoride membrane (Bio-Rad, Hercules, CA) with a semidry apparatus. The membrane was probed with the anti-ARF6 monoclonal antibody and visualized by chemiluminescence (Renaissance Western blot chemiluminescence reagent, PerkinElmer Life Sciences) with the use of horseradish peroxidase conjugated anti-mouse IgG as a second antibody.

Immunostaining—The isolated glands were fixed with 10% formalin, permeabilized with 0.1% Triton X-100, and incubated with anti-ARF6 monoclonal antibody (1:30) or anti-H^+,K^+-ATPase α-subunit rat polyclonal antibody (7). These glands were visualized by Cy3-anti-mouse IgG (1:50) and fluorescein isothiocyanate-anti-rat IgG (1:100), and examined by microscopy (Nikon Eclipse TE300) using a confocal laser scanning system (μRadiance, Bio-Rad). Negative controls using control mouse IgG as the first antibody showed signals lower than the detection limit under the conditions presently employed.

Cell Culture—Gastric glands were cultured basically according to the method described by Chew *et al.* (13) with slight modifications (14). Isolated gastric glands were washed four times and incubated for 10 min in medium B (Dulbecco's modified Eagle's medium/F-12, 2 mg/ml bovine serum albumin, 10 mM glucose, 100 μg/ml gentamicin, pH 7.4) plus 25 μg/ml amphotericin B, to prevent yeast infection. After the glands were washed once in medium A (medium B plus 8 nM EGF, 10 nM hydrocortisone, 800 nM insulin, 3.1 nM sodium selenite, 2.6 μg/ml transferrin, 0.93 μg/ml ethanolamine, 5 μg/ml Geneticin, 8 μg/ml amphotericin B), glands were incubated for 30 min in 10% fetal bovine serum/Dulbecco's modified Eagle's medium-pre coated flask to exclude fibroblasts. Plating onto Matrigel (Collaborative Biomedical, diluted 1:7)-coated coverslips followed, and cells were thereafter incubated at 37 °C in culture medium A.

Construction and Use of ARF6 Adenovirus—ARF6-HA (wild type, Q67L, N122I) plasmids in pcDNA3 were used to create a recombinant adenovirus with the AdEasy vector system (15). First, the ARF6-HA cDNA was isolated from its plasmid by *Hin*dIII and *Xba*I, and the insert DNA was ligated into the pShuttle-CMV plasmid. This pShuttle-CMV: ARF6-HA recombinant plasmid was linearized and recombined with the pAdEasy plasmid in *Escherichia coli*. Purified pAdEasy:ARF6-HA plasmids were then digested with *Pac*I endonuclease and transfected into low passage HEK293 cells using SuperFect transfection reagent (Qiagen). Control cells were infected with vector expressing enhanced green fluorescent protein (EGFP). The cultured gastric glands (3.5×10^4 cells/well) were infected with viruses at a multiplicity of infection of 300. Forty hours after infection, the cells were used for aminopyrine uptake assay (14).

Statistical Analysis—Parametric data are expressed as means ± S.E. Multiple comparisons were analyzed by analysis of variance and Fisher's post hoc test with the use of a computer program (Super ANOVA, Abacus Concepts, Berkeley, CA). The level of significance was set at $p < 0.05$.

RESULTS

Effects of GTP and GTPγS on Gastric Acid Secretion in β-Escin-permeabilized Gastric Glands—As shown in Fig. 1, we found that GTP in the range of 0.3–3 mM dose-dependently stimulated aminopyrine accumulation in β-escin-permeabilized gastric glands. The secretagogue effect of 100 μM cAMP was completely inhibited by 100 μM GTPγS. These data indicate that one or more G proteins, of which the GTP hydrolysis cycle is essential for activation, are involved in acid secretion.

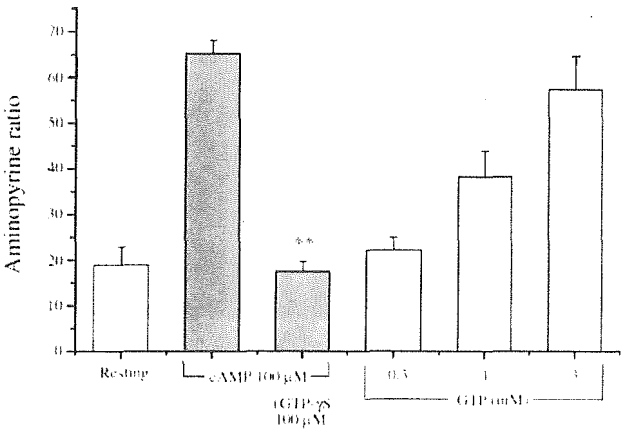

FIG. 1. **Opposite effects of GTP and GTPγS on [^{14}C] aminopyrine accumulation in β-escin-permeabilized gastric glands.** Gastric glands were permeabilized with 50 μM β-escin, and aliquots were assayed for aminopyrine accumulation for 30 min at 37 °C in the presence of indicated secretagogues. Values are means ± S.E. of three to four experiments performed in a duplicate manner. **, significantly different from cAMP alone at $p < 0.01$.

Cellular Localization of ARF6 in Gastric Glands—If ARF6 has a role in regulation of membrane traffic and acid secretion in gastric parietal cell, it should exist in the cell. Rabbit isolated gastric glands were incubated with 100 μM cimetidine (resting) or 100 μM histamine plus 30 μM isobutylmethylxanthine (maximally stimulated), fixed with formalin, and stained with anti-ARF6 monoclonal antibody (Fig. 2). ARF6 mainly located in parietal cells, but not in chief cells, in the gastric gland. Within the parietal cell, ARF6 showed a relatively even distribution (with little membranous structure) in the resting state, whereas it took a more membranous appearance upon stimulation. This point will be developed in the following section. We also concluded that any changes in ARF6 could be interpreted as changes in parietal cells even when using the heterogenous preparation of gastric glands.

To determine the intracellular distribution of ARF6, gastric glands were homogenized and fractionated into apical membrane-rich, tubulovesicle-rich, and cytosolic fractions followed by immunoblotting using anti-ARF6 antibody (Fig. 3). Since Gaschet and Hsu (16) reported that the intracellular distribution of ARF6 between membrane and cytosol was sensitive to the concentration of Mg^{2+}, we used either Mg^{2+}-containing or Mg^{2+}-free EDTA-containing buffer for homogenization. ARF6 was harvested mainly (~70%) in the cytosolic fraction in Mg^{2+}-containing buffer, whereas in Mg^{2+}-free buffer, it distributed to the membrane fractions. The content of ARF6 was increased 2-fold in the tubulovesicles, whereas that was 3-fold in the apical membrane, suggesting its preference to the latter. To confirm this observation, we performed immunohistochemistry of β-escin-permeabilized gastric glands. In the presence of Mg^{2+}, ARF6 showed a diffuse staining pattern in the cytosol of parietal cell (Fig. 4*A*). Because Mg^{2+} concentration in mammalian cells is approximately a few millimolar, this staining pattern of ARF6 could reflect physiological localization. When the permeabilized glands were treated with membrane-impermeable Mg^{2+} chelator, *trans*-1,2-diaminocyclohexane-*N*,*N*,*N*′,*N*′-tetraacetic acid (CDTA), the staining of ARF6 appeared to accumulate in the membranous structure, and that is characteristic for apical intracellular canaliculi (Fig. 4*B*, *arrows*).

In the next experiment, we examined the distribution of ARF6 in the presence or absence of 100 μM GTPγS. In this

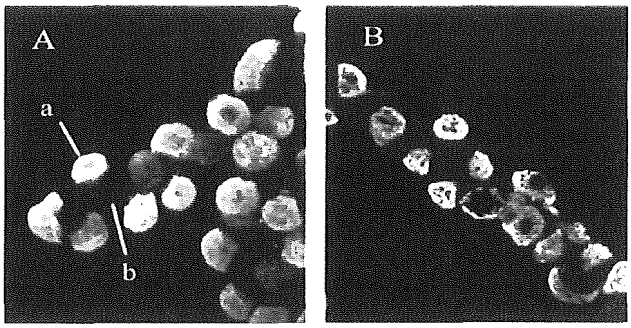

FIG. 2. **Cellular localization of ARF6 in rabbit gastric glands.** Isolated rabbit gastric glands were fixed, permeabilized, and probed with anti-ARF6 monoclonal antibody (1/30). The first antibody was visualized by Cy3-anti-mouse antibody (1/50). *A*, resting rabbit gastric gland (incubated with 100 μM cimetidine for 15 min at 37 °C) with the positions of parietal cell (*a*) and chief cell (*b*) are shown. Note that ARF6 is almost exclusively exists in parietal cell. *B*, stimulated gastric gland (incubated with 100 μM histamine plus 30 μM isobutylmethylxanthine for 15 min at 37 °C) is shown. Note that the staining pattern of ARF in stimulated parietal cell appears more membranous than that in resting ones.

assay, we incubated and homogenized gastric glands using Mg^{2+}-containing buffer. When treated with GTPγS, cytosolic ARF6 decreased and mainly translocated to the tubulovesicular compartment, but not to the apical membrane, in contrast to the Mg^{2+}-free condition (Fig. 5, *A* and *B*). We tried to confirm this result by immunohistochemistry. As expected from the biochemical data, it was observed that the staining pattern with anti-ARF6 was quite similar to that with anti-H,K-ATPase α-subunit, the tubulovesicle marker protein, in permeabilized, GTPγS-treated glands (Fig. 6).

ARF6 Translocates to the Intracellular Canaliculi Together with H^+,K^+-ATPase in Secretagogue-stimulated Gastric Parietal Cells—Resting (incubated with 100 μM cimetidine for 30 min) or maximally stimulated (incubated with 100 μM histamine plus 30 μM isobutylmethylxanthine) gastric glands were double-stained with anti-ARF6 and anti-H^+,K^+-ATPase α-subunit. Under the resting condition, both ARF6 and H^+,K^+-ATPase appeared to be diffusely distributed in cytosol, whereas the merged image showed little co-localization of these proteins (Fig. 7, *A–C*). This observation is consistent with the result of biochemical data, *i.e.* ARF6 distributed to cytosol, whereas H^+,K^+-ATPase mainly existed in tubulovesicles (which appeared to be diffuse under light microscopy). When the glands were stimulated, H^+,K^+-ATPase translocated to the intracellular canaliculi (Fig. 7, *D–F*). The staining pattern of ARF6 became similar to that of H^+,K^+-ATPase, and this was evident from the merged image. We suggest that ARF6 translocated to the apical membrane together with H^+,K^+-ATPase when parietal cell was stimulated.

Effects of Myristoylated N-terminal Peptide of ARF on Acid Secretion—To investigate whether ARF6 directly regulates acid secretion, we tested the effect of N-terminal peptide of ARF6 on aminopyrine accumulation of rabbit isolated glands. Because the N-terminal of small G proteins is thought to interact with the effectors and the interaction was expected to occur within membranes, we obtained the myristoylated synthetic N-terminal peptide of ARF6 (myr-GKVLSKIFGNKE) (17). Gastric glands were permeabilized with 50 μM β-escin, and aliquots were assayed for aminopyrine accumulation for 30 min at 37 °C. As shown in Fig. 8, the aminopyrine ratio stimulated by 3 mM GTP was significantly inhibited by the peptide at 30 μM. In contrast, myristoylated peptide with reversed sequence, myr-EKNGFIKSLVKG, used as a negative control, failed to affect the aminopyrine ratio.

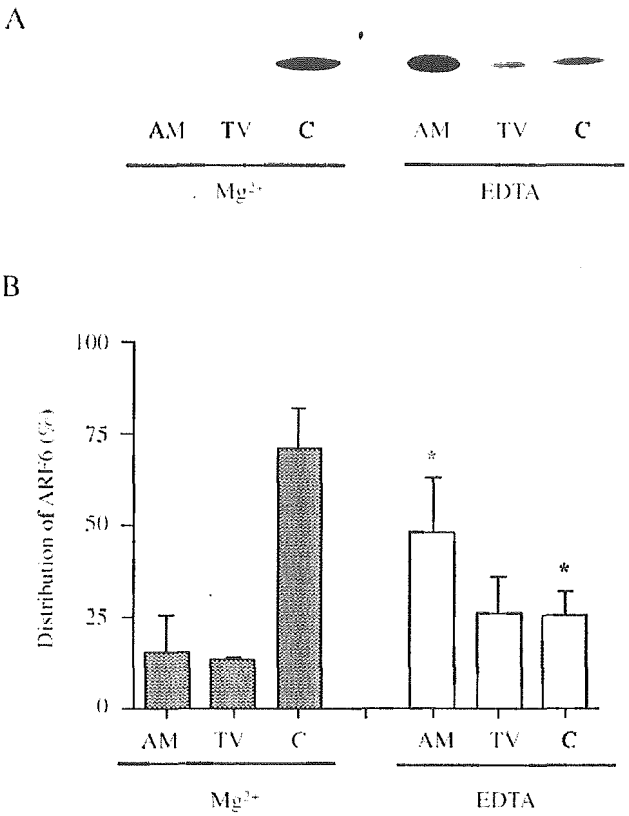

FIG. 3. **Subcellular distribution of ARF6.** Gastric glands were homogenized either in the presence of Mg^{2+} (2.5 mM) or EDTA (0.5 mM). The homogenate was fractionated into apical membrane-rich (*AM*), tubulovesicle-rich (*TV*), and cytosolic (*C*) fractions followed by immunoblotting using anti-ARF6 antibody. The amount applied to the gel was set proportional to the suspended sample volume such that the density of the bands expressed the distribution within the total. *A*, a representative blot showing ARF6-positive bands. *B*, the bands on the blot were quantified by the densitometry and expressed as the % of total (n = 3, mean ± S.E.). Note that ARF6 mainly distributes to the soluble, cytosolic fraction in Mg^{2+}-containing buffer, whereas in Mg^{2+}-free buffer, it moved to the membrane fraction, the apical membrane-rich, rather than tubulovesicle-rich fraction. *, significantly different from corresponding control value (Mg^{2+}-containing) at $p < 0.05$.

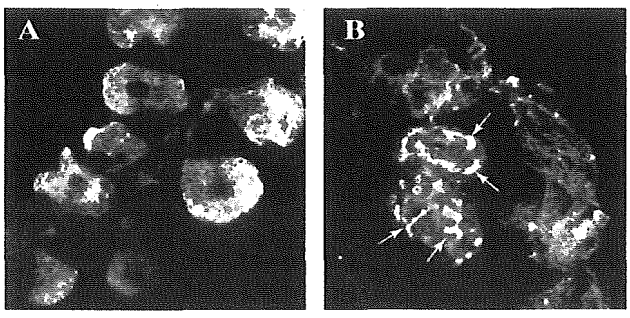

FIG. 4. **Mg^{2+} chelation changes in localization of ARF6 in rabbit gastric glands.** β-Escin-permeabilized gastric glands were incubated, fixed, and probed by the same protocol as in Fig. 2. *A*, resting (incubated with 100 μM cimetidine for 15 min at 37 °C) glands are shown. *B*, glands incubated with 5 mM CDTA for 15 min at 37 °C are shown. It appears that ARF6 translocates to the intracellular canaliculi (*arrows*) by CDTA treatment. Due to the treatment with β-escin, the preservation of the gland structure is inferior to that of intact glands.

Effects of Expression of ARF6 and Its Mutants on Aminopyrine Accumulation in Cultured Gastric Glands—To investigate the direct role of ARF6 in acid secretion, we constructed adeno-

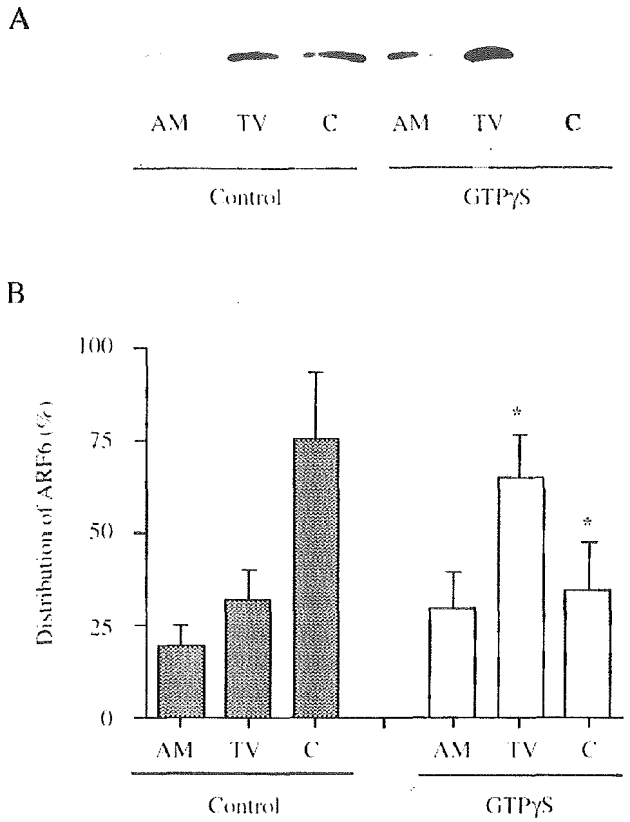

FIG. 5. **Redistribution of ARF6 in gastric glands with GTPγS.** β-Escin-permeabilized gastric glands were incubated in high K^+ buffer in the presence (+) or absence (−) of 100 μM GTPγS (37 °C, 15 min), homogenized in Mg^{2+}-containing buffer, and fractionated into apical membrane-rich (*AM*), tubulovesicle-rich (*TV*), and cytosolic (*C*) fractions followed by immunoblotting using anti-ARF6 antibody. *A*, a representative blot showing ARF6-positive bands. *B*, the bands on the blot were quantified by the densitometry and expressed as the % of total ($n = 3$, mean ± S.E.). Note that ARF6 in the cytosolic fraction moved to the tubulovesicle-rich, rather than the apical membrane-rich, fraction by the treatment with GTPγS. *, significantly different from corresponding control value at $p < 0.05$.

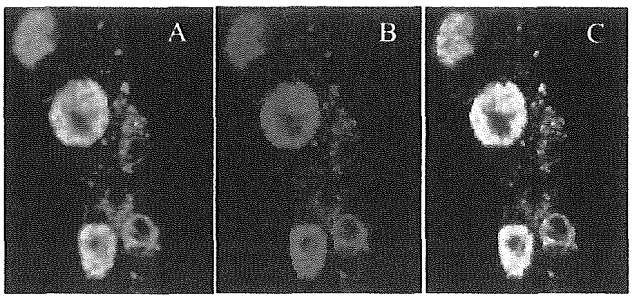

FIG. 6. **Co-localization of ARF6 and H^+,K^+-ATPase in β-escin-permeabilized, GTPγS-treated rabbit gastric glands.** Isolated glands, permeabilized with β-escin, were treated with 100 μM GTPγS (37 °C, 15 min), fixed, and stained for ARF6 (*green*, *A*) and H^+,K^+-ATPase (*red*, *B*). Stainings of both ARF6 and H^+,K^+-ATPase, the marker enzyme of tubulovesicles, appear diffuse but show some membranous structure in the cytosol of parietal cell. The *merged image* (*C*) shows that most of these two proteins are co-localized, suggesting that ARF6 is present on tubulovesicular membranes in GTPγS-treated parietal cells.

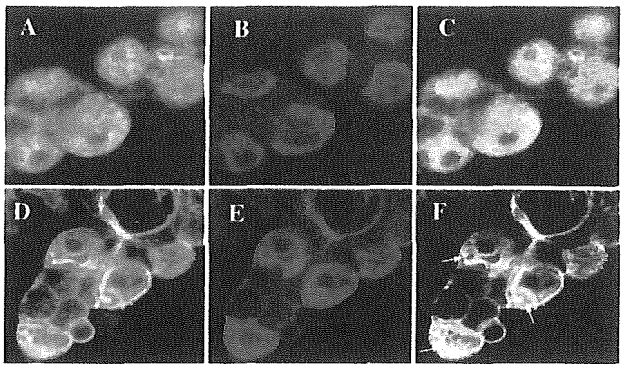

FIG. 7. **Redistribution of H^+,K^+-ATPase and ARF6 in association with stimulation of rabbit gastric glands.** Resting isolated glands (treated with 100 μM cimetidine) were fixed, permeabilized, and stained for ARF6 (*green*, *A*) and H^+,K^+-ATPase (*red*, *B*). The *merged image* (*C*) shows that both ARF6 and H^+,K^+-ATPase are diffusely present in the cytosol of parietal cell and that their co-localization was relatively poor. When the glands were stimulated with 100 μM histamine plus 30 μM IBMX (15 min at 37 °C) and stained for ARF6 (in *green*, *D*) and H^+,K^+-ATPase (*red*, *E*), it was obvious from the *merged image* (*F*) that both proteins considerably co-localized, especially at the intracellular canaliculi (*arrows*) of the parietal cell.

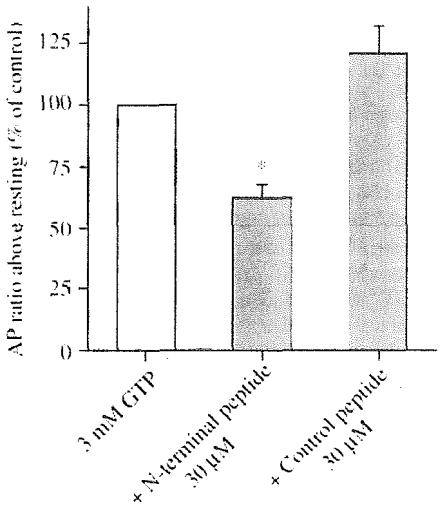

FIG. 8. **Effects of myristoylated peptides on [^{14}C]aminopyrine accumulation in β-escin-permeabilized gastric glands.** Gastric glands were permeabilized with 50 μM β-escin and stimulated with 3 mM GTP at 37 °C for 30 min. Acid secretion was monitored by [^{14}C]aminopyrine accumulation. Aminopyrine ratio above resting (100 μM cimetidine alone) was calculated and expressed as the percentage of stimulated value (cimetidine plus 3 mM GTP). Myristoylated N-terminal peptide of ARF6 (myr-GKVLSKIFGNKE) and its negative control with reversed sequence (myr-EKNGFIKSLVKG) were both used at 30 μM. Values are means ± S.E. of three separate experiments. *, significantly different from control at $p < 0.05$.

viruses, *i.e.* HA-tagged ARF6 wild type (WT) and its mutants (Q67L, and N122I), which were transiently expressed in cultured gastric glands. The expression of each mutant was estimated to be more than 10 times as much as the endogenous ARF6 assessed by immunoblotting (data not shown). The acid secretion was monitored by [^{14}C]aminopyrine accumulation, and the results are shown in Fig. 9. ARF6 Q67L, a GTP hydrolysis-deficient, constitutive active mutant, significantly reduced acid secretion, whereas N122I, a mutant defective in GTP binding, tended to inhibit secretion but was not statistically significant.

DISCUSSION

At present, the generally accepted model for vesicular fusion events essential for acid secretory process includes rab family proteins, especially rab11a. There is no doubt of the importance of rab11a, because: (*a*) rab11a exists on the tubulovesicular

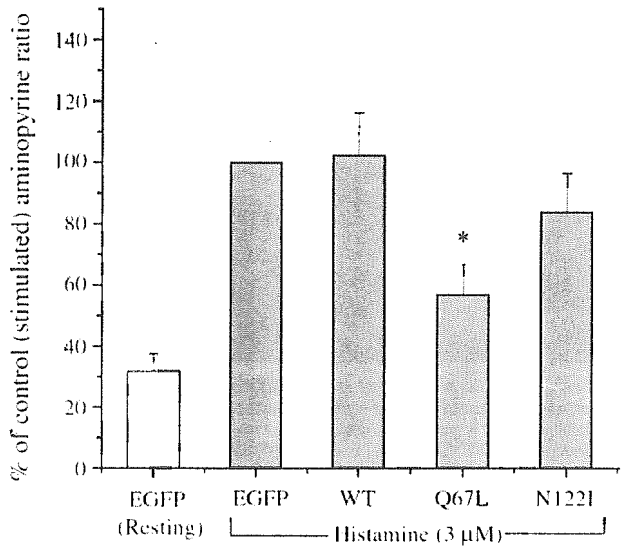

FIG. 9. Effects of expression of ARF6 mutants on [^{14}C]aminopyrine accumulation in cultured gastric glands. Gastric glands were cultured and infected with adenoviruses carrying wild type ARF6 (*WT*), GTPase-defective mutant (*Q67L*), GTP-binding defective mutant (*N122I*), as described under "Experimental Procedures" (multiplicity of infection = 300). [^{14}C]Aminopyrine uptake was used to assess acid secretion. Data are expressed as values relative to histamine (3 μM)-stimulated cells expressing EGFP. Values are means ± S.E. of five separate experiments. *, significantly different from control at $p < 0.05$.

membrane, (*b*) it translocates to the apical secretory membrane together with the proton pump, and (*c*) the dominant negative mutant of rab11a inhibits acid secretion (18, 19). However, there has been some evidence that another small G protein might be involved in the process: Miller and Hersey (4) reported that GTPγS acted as a potent inhibitor of acid secretion in α-toxin-permeabilized gastric glands. We also confirmed their results by using the β-escin-permeabilized gland model and observed that translocation of tubulovesicles to the apical membrane was inhibited by GTPγS, suggesting that one of the sites of action of GTPγS is the fusion events (or earlier) in the sequence of activation (5). It was also observed that ARF-like immunoreactivity accumulated in the membrane fraction of GTPγS-treated glands using non-selective anti-ARF antibody (5). In the same report, we applied various functional peptides, including rab and ARF, and found that the N-terminal peptide of ARF 1, but not of rab, showed biological activity, *i.e.* inhibition of acid secretion (5).

In the present study, we observed that GTP by itself behaved as an agonist for acid secretion in permeabilized glands and that the stimulatory effect of cAMP was abolished by GTPγS. The inhibitory effect of GTPγS cannot be explained by the involvement of rab members, because GTPγS works as an agonist for most small G proteins in the secretory process. In fact, GTPγS stimulates pepsinogen secretion from chief cells that are also contained in the gastric gland (4). Our results in turn clearly indicate a possible involvement of ARF family members in acid secretion, because ARF is the only family on which GTPγS causes an inhibitory effect in the process involved (3). Because brefeldin A, an ARF-GEF inhibitor, was ineffective in acid secretion (5), only ARF6, of which GEF is known to be insensitive, remained as a candidate. In the day when these experiments were done, it was considered that ARF6 was a permanent resident on the membrane, and its localization was unaffected by GTPγS. Therefore, we were reluctant to conclude that ARF6 is involved in acid secretion. However, it was recently revealed that ARF6 exists in both soluble and membrane-bound forms similar to other ARF family proteins (16, 20). We then embarked on the present study to elucidate whether ARF6 is involved in the acid secretory process.

ARF activity appears to be regulated by guanine nucleotide exchange and hydrolysis like other small G proteins, because cytosolic ARF is in a GDP-bound state, and it is GTP-bound ARF that associates with cellular membranes (21). It was reported that, unlike other ARF, membrane distribution of ARF6 expressed in various cell lines is affected by Mg^{2+} concentration (16). In gastric glands, ARF6 mainly exists in parietal cells and is located in both cytosol and membrane fractions in the presence of physiological concentration of Mg^{2+} (2.5 mM). In the EDTA- or CDTA-containing buffer, it translocated from cytosol to intracellular canaliculi. Gaschet and Hsu (16) postulated that the translocation is due to the Mg^{2+} dependence of GAP activity specific for ARF6 on the membrane, *i.e.* removal of Mg^{2+} results in loss of GAP activity to hold ARF-GTP in the membrane. According to their interpretation, ARF6 existing in the cytosol in the GDP form moves to the apical membrane in an activated GTP-binding form and goes back to cytosol when GTP hydrolysis is activated by GAP on the membrane.

The GTPγS-dependent recruitment of ARF6 from cytosol to the vesicular compartment supports the GTPase cycle-dependent translocation of ARF6 in parietal cell. In several secretory cells, GTPγS-dependent translocation of ARF to secretory granules has also been observed (25). However, it is presently unclear why ARF6 distributes to different membrane compartments, *i.e.* to the apical membrane by Mg^{2+} chelator and to the tubulovesicles by GTPγS in parietal cell. It could be possible that the Mg^{2+} sensitivity of GAP is different between these membranes or that the effect of Mg^{2+} chelating is not related to GAP but to another unknown mechanism. In any case, it could be concluded that ARF6 redistributes among cytosol, tubulovesicles, and apical secretory membranes depending upon its GTPase activity. In intact, highly stimulated parietal cells, ARF6 and H^+,K^+-ATPase co-localized on the apical intracellular canaliculi. Based on these data, the whole scenario would be that the activated GTP-bound form of ARF6 binds to tubulovesicular membrane, and subsequently this ARF6-tubulovesicle complex translocates to the apical membrane.

In addition to its translocation within parietal cell, ARF6 appears to play a role in acid secretion. In the present study, the myristoylated N-terminal fragment of ARF6, but not its reversed sequence, partially inhibited GTP-stimulated acid secretion in permeabilized glands. To confirm this, we employed an expression system using adenovirus as more specific probes. It was found that expression of ARF6Q67L, a GTP hydrolysis-deficient mutant, and not the wild type of ARF, inhibited histamine-induced acid secretion. This strongly supports our hypothesis that the GTP-hydrolysis cycle of ARF6 is essential for acid secretion. There have been several reports that overexpression of wild type ARF6 does not affect the physiological functions in which ARF6 was proved to be involved (23, 24). Zhang *et al.* (25) reported that constitutive active ARF1 (Q71L) caused vesiculation of the Golgi apparatus and expansion of the ER lumen, leading to inhibition of constitutive protein secretion in NRK cells. Although the mechanism whereby GTP-bound ARF inhibits secretion has not been fully elucidated, it is postulated that continuous association of ARF with specific membrane components arrests the events of membrane fusion (26). Considering the observation that ARF6 was accumulated in the tubulovesicular compartment in the presence of GTPγS, it could be postulated that GTP-bound ARF6 translocates to tubulovesicles from cytosol, and also, if GTP hydrolysis is obstructed on the membrane, ARF6-tubulovesicle complex cannot

translocate to the apical membrane. Myristoylated N-terminal fragment of ARF6 might weakly mimic this process with its accessibility to the membranes in parietal cell.

We have recently demonstrated that phosphatidylinositol 4,5-bisphosphate ($PI(4,5)P_2$) and its carrier, phosphatidylinositol transfer protein, are essential components for acid secretion (27, 28). It was reported that ARF6 increased $PI(4,5)P_2$ production through activation of phospholipase D (29) or phosphatidylinositol-4-phosphate 5-kinase α (30). Therefore, it would be reasonable to postulate that ARF6 works by producing $PI(4,5)P_2$, which is a key regulator of both membrane traffic and proton pumping in parietal cell. Obviously, further study is needed to elucidate the link between activation of protein kinase A and ARF6, as well as that between ARF6 and fusion events in parietal cell.

The main point of the present study is that we propose a reasonable answer for the long standing riddle: the potent inhibitory effect of GTPγS on acid secretion. This successfully clarifies the important role of ARF6 in the physiologically normal cell, *i.e.* acutely isolated or primary cultured parietal cell, not in the transformed cell lines.

REFERENCES

1. Urushidani, T., and Forte, J. G. (1997) *J. Membr. Biol.* **159,** 99–111
2. Okamoto, C. T., and Forte, J. G. (2001) *J. Physiol.* **532,** 287–296
3. Takai, Y., Sasaki, T., and Matozaki, T. (2001) *Physiol. Rev.* **81,** 153–208
4. Miller, M. D., and Hersey, S. J. (1996) *Am. J. Physiol.* **270,** G962–G968
5. Akagi, K., Nagao, T., and Urushidani, T. (1999) *Am. J. Physiol.* **277,** G736–G744
6. Chavrier, P., and Goud, B. (1999) *Curr. Opin. Cell Biol.* **11,** 466–475
7. Muto, Y., Nagao, T., Yamada, M., Mikoshiba, K., and Urushidani, T. (2001) *Am. J. Physiol.* **280,** C155–C165
8. Hosaka, M., Toda, K., Takatsu, H., Torii, S., Murakami, K., and Nakayama, K. (1996) *J. Biochem. (Tokyo)* **120,** 813–819
9. Toda, K., Nogami, M., Murakami, K., Kanaho, Y., and Nakayama, K. (1999) *FEBS Lett.* **442,** 221–225
10. Berglindh, T. (1990) *Methods Enzymol.* **192,** 93–107
11. Urushidani, T., and J Forte, J. G. (1987) *Am. J. Physiol.* **252,** G458–G465
12. Laemmli, U. K. (1970) *Nature* **227,** 680–685
13. Chew, C. S., Ljungstroem, M., Smolka, A., Smolka, A., and Brown, M. R. (1989) *Am. J. Physiol.* **256,** G254–G263
14. Tashiro, K., Nagao, T., Kurose, H., Ichijo, H., and Urushidani, T. (2003) *J. Cell. Physiol.*, in press
15. He, T. C., Zhou, S., da Costa, L. T., Yu, J., Kinzler, K. W., and Vogelstein, B. (1998) *Proc. Natl. Acad. Sci. U. S. A.* **95,** 2509–2514
16. Gaschet, J., and Hsu, V. W. (1999) *J. Biol. Chem.* **274,** 20040–20045
17. Mukherjee, S., Gurevich, V. V., Jones, J. C. R., Casanova, J. E., Frank, S. R., Maizels, E. T., Bader, M.-F., Kahn, R. A., Palczewski, K., Aktories, K., and Hunzicker-Dunn, M. (2000) *Proc. Natl. Acad. Sci. U. S. A.* **97,** 5901–5906
18. Calhoun, B. C., Lapierre, L. A., Chew, C. S., and Goldenring, J. R. (1998) *Am. J. Physiol.* **275,** C163–C170
19. Duman, J. G., Tyagarajan, K., Kolsi, M. S., Moore, H. P., and Forte, J. G. (1999) *Am. J. Physiol.* **277,** C361–C372
20. Yang, C. Z., Heimberg, H., D'Souza-Schorey, C., Mueckler, M. M., and Stahl, P. D. (1998) *J. Biol. Chem.* **273,** 4006–4011
21. Walker, M. W., Bobak, D. A., Tsai, S. C., Moss, J., and Vaughan, M. (1992) *J. Biol. Chem.* **267,** 3230–3235
22. Dohke, Y., Hara-Yokoyama, M., Fujita-Yoshigaki, J., Kahn, R. A., Kanaho, Y., Hashimoto, S., Sugiya, H., Furuyama, S. (1998) *Arch. Biochem. Biophys.* **357,** 147–154
23. Dana, R. R., Eigsti, C., Holmes, K. L., and Leto, T. L. (2000) *J. Biol. Chem.* **275,** 32566–32571
24. Vitale, N., Chasserot-Golaz, S., Bailly, Y., Morinaga, N., Frohman, M. A., and Bader, M.-F. (2002) *J. Cell Biol.* **159,** 79–89
25. Zhang, C. J., Rosenwald, A. G., Willingham, M. C., Skuntz, S., Clark, J., and Kahn, R. A. (1994) *J. Cell Biol.* **124,** 289–300
26. Jones, A. T., Spiro, D. J., Kirchhausen, T., Melancon, P., and Wessling-Resnick, M. (1999) *J. Cell Sci.* **112,** 3477–3485
27. Akagi, K., Nagao, T., and Urushidani, T. (2001) *J. Biol. Chem.* **276,** 28171–28178
28. Omi, N., Nagao, T., and Urushidani, T. (2001) *Am. J. Physiol.* **281,** G786–G797
29. Liscovitch, M., Czarny, M., Fiucci, G., and Tang, X. (2000) *Biochem. J.* **345,** 401–415
30. Honda, A., Nogami, M., Yokozeki, T., Yamazaki, M., Nakamura, H., Watanabe, H., Kawamoto, K., Nakayama, K., Morris, A. J., Frohman, M. A., and Kanaho, Y. (1999) *Cell* **99,** 521–532

Available online at www.sciencedirect.com
SCIENCE DIRECT®
Leukemia Research 29 (2005) 1095–1096
Leukemia Research
www.elsevier.com/locate/leukres

Letter to the Editor

Bone marrow cells of myelodysplastic syndromes exhibit significant expression of apollon, livin and ILP-2 with reduction after transformation to overt leukemia

Bone marrow cells of patients with myelodysplastic syndromes (MDS) frequently undergo apoptosis, though the apoptotic cell ratio decreases when overt leukemia (OL) develops. Using bone marrow samples from control, MDS, OL transformed from MDS (MDS → OL), and de novo AML subjects, we have compared the expression of the inhibitor of apoptosis protein (IAP) gene family proteins including survivin, cIAP1, cIAP2, NAIP and XIAP by the quantitative real time RT-PCR method [1]. Overexpression of mRNA for survivin, cIAP1, NAIP and XIAP was significant in MDS bone marrow cells compared with control samples. However, the expression of mRNA for survivin, cIAP1 and cIAP2 exhibited a remarkable decrease after the development of OL (MDS → OL). Next, the chronological changes in the expression of IAPs were determined in cases of MDS with evolution of OL. Although the expression of cIAP1 and cIAP2 revealed a sudden or gradual decrease as OL developed, survivin in many cases and XIAP in the majority of cases exhibited a peak of expression before a decline, indicating that these IAPs could be associated with the early events in the development of OL.

We would like to extend the study to reveal the expression of recently identified IAPs including apollon [2], livin [3] and IAP-like protein 2 (ILP-2) [4] in these samples by the quantitative real time RT-PCR method (Fig. 1). Although mechanisms of action for these new IAP molecules are not completely clarified, overexpression of these molecules induced various degree of anti-apoptotic signaling [2–4].

The expression of mRNA for apollon in MDS bone marrow was significantly higher than that of control subjects ($p < 0.05$ by Mann–Whitney's U-test), whereas the expression significantly reduced when overt leukemia developed ($p < 0.05$ by Wilcoxon's test). In contrast, de novo AML bone marrow exhibited the significantly higher expression than MDS → OL subjects ($p < 0.01$).

The expression of livin in MDS was relatively higher than control and the expression significantly reduced in MDS → OL subjects ($p < 0.05$). De novo AML samples showed significantly higher expression than control ($p < 0.05$) and MDS → OL subjects ($p < 0.05$).

The expression of ILP-2 in MDS and de novo AML exhibited significantly higher expression than control ($p \lesssim 0.01$, respectively). Although the differences were not significant, the expression in MDS → OL subjects was relatively lower than MDS and de novo AML subjects.

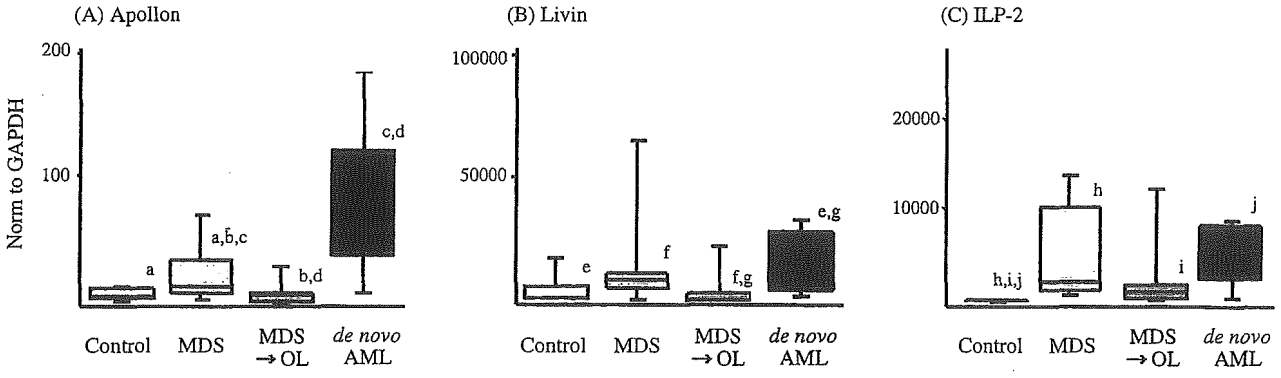

Fig. 1. Quantitative RT-PCR analysis of IAP family proteins, apollon, livin and ILP-2 in control ($n = 5$), MDS ($n = 9$), MDS → OL ($n = 9$) and de novo AML cases ($n = 5$). Relative intensity was calculated as (intensity of reaction of IAP family [total Raji RNA, ng])/(intensity of reaction of GAPDH [total Raji RNA, ng]). The box plot graphs indicate the values for MDS and AML cases. Bars indicate 90% tile and 10% tile and boxes indicate 75% tile to 25% tile. Differences were significant between the samples as follows using Wilcoxon's test (comparison of MDS and MDS → OL) or Mann–Whitney's U-test (comparison between other combinations): apollon, control and MDS ($^a p < 0.05$), MDS and MDS → OL ($^b p < 0.05$), MDS and de novo AML ($^c p < 0.05$), and MDS → OL and de novo AML ($^d p < 0.01$); livin, control and de novo AML ($^e p < 0.05$), MDS and MDS → OL ($^f p < 0.05$), and MDS → OL and de novo AML ($^g p < 0.05$); ILP-2, control and MDS ($^h p < 0.01$), control and MDS → OL ($^i p < 0.01$), and control and de novo AML ($^j p < 0.01$).

doi:10.1016/j.leukres.2005.02.004

In summary, these results indicate that apollon, livin and ILP-2 would not serve as the major inhibitor/regulator of apoptosis in MDS as well as in MDS → OL, because highly apoptotic bone marrow (MDS) exhibit higher expression of these molecules in contrast that lower apoptotic bone marrow (MDS → OL) exhibit lower expression. However, we cannot ignore the possibility that these molecules were transiently overexpressed at the very early stage of leukemic transformation and work as the trigger for inhibition of apoptosis such as survivin and XIAP [1]. By contrast, these IAPs could have anti-apoptotic roles in the de novo AML bone marrow. The differential expression manner of apollon, livin and ILP-2 between MDS → OL and de novo AML would be derived from the different biological character of these myeloid leukemias, might serve as a clue to clarify the mechanisms for chemotherapy-resistant nature of MDS → OL, and could be useful for the differential diagnosis of AML transformed from MDS and de novo AML.

Acknowledgements

This work was supported in part by a grant-in-aid from the Ministry of Education, Culture, Sports, Science and Technology of Japan (No. 14570180).

References

[1] Yamamoto K, Abe S, Nakagawa Y, Suzuki K, Hasegawa M, Inoue M, et al. Expression of IAP family proteins in myelodysplastic syndromes transforming to overt leukemia. Leuk Res 2004;28:1203–11.

[2] Chen Z, Naito M, Hori S, Mashima T, Yamori T, Tsuruo T. A human IAP-family gene, apollon, expressed in human brain cancer cells. Biochem Biophys Res Commun 1999;264:847–54.

[3] Vucic D, Stennicke HR, Pisabarro MT, Salvesen GS, Dixit VM. ML-IAP, a novel inhibitor of apoptosis that is preferentially expressed in human melanomas. Curr Biol 2000;10:1359–66.

[4] Shin H, Renatus M, Eckelman BP, Nunes VA, Sampaio CA, Salvesen G. The BIR domain of IAP-like protein 2 is conformationally unstable: implications for caspase inhibition. Biochem J 2005;385: 1–10.

S. Abe
K. Yamamoto
M. Hasegawa
M. Inoue
M. Kurata
K. Hirokawa
M. Kitagawa*
Department of Comprehensive Pathology Aging and Developmental Sciences Tokyo Medical and Dental University Graduate School, Tokyo 113-8519, Japan

Y. Nakagawa
K. Suzuki
Department of Hematology, Japanese Red Cross Medical Center, Tokyo 150-8935, Japan

* Corresponding author. Tel.: +81 3 5803 5399
fax: +81 3 5803 0123
E-mail address: masa.pth2@med.tmd.ac.jp
(M. Kitagawa)

27 January 2005
Available online 16 March 2005

Available online at www.sciencedirect.com
SCIENCE DIRECT®
Leukemia Research 29 (2005) 933–942
Leukemia Research
www.elsevier.com/locate/leukres

Resistance against Friend leukemia virus-induced leukemogenesis in DNA-dependent protein kinase (DNA-PK)-deficient *scid* mice associated with defective viral integration at the *Spi-1* and *Fli-1* site

Maki Hasegawa [a], Shuichi Yamaguchi [a], Shiro Aizawa [b], Hidetoshi Ikeda [c], Kouichi Tatsumi [b], Yuko Noda [b], Katsuiku Hirokawa [a], Masanobu Kitagawa [a,*]

[a] *Department of Comprehensive Pathology, Aging and Developmental Sciences, Tokyo Medical and Dental University, Graduate School, 1-5-45 Yushima, Bunkyo-ku, Tokyo 13-8519, Japan*
[b] *Research Center for Radiation Safety, National Institute of Radiological Sciences, 4-9-1 Anagawa, Inage-ku, Chiba 263-8555, Japan*
[c] *Laboratory of Infectious Diseases, National Institute of Animal Health, 3-1-5 Kannondai, Tsukuba City, Ibaraki 305-0856, Japan*

Received 5 October 2004; accepted 22 January 2005
Available online 11 March 2005

Abstract

Retroviral DNA integration is mediated by the viral protein integrase. However, elements of the host DNA repair machinery such as the phosphatidylinositol 3-kinase (PI-3K)-related protein kinase family system would play a role in the integration of viral DNA into the host DNA. Here, we show that a host PI-3K-related protein kinase, DNA-dependent protein kinase (DNA-PK), plays a role in the specific integration of retroviral DNA and induction of retroviral diseases in vivo. DNA-PK-deficient *scid* mice inoculated with Friend leukemia virus (FLV) exhibited a random integration into their genomic DNA and expressed the viral envelope protein gp70. However, the specific integration of FLV at *Spi-1* or *Fli-1* sites did not occur in association with the significant resistance of *scid* mice to FLV-induced leukemogenesis. In contrast, the knockout of another member of the PI-3K-related protein kinase family, encoded by the *ataxia telangiectasia mutated* (*ATM*) gene, resulted in mice as sensitive to FLV-induced leukemogenesis as the wild type mice. FLV was specifically integrated into the DNA at *Spi-1* and *Fli-1* sites with significant expression of these transcription factors. These findings indicated that DNA-PK would be essential for controlling the in vivo integration of FLV at specific sites as well as the susceptibility to FLV-induced leukemogenesis.

Keywords: Retrovirus infection; Friend virus; DNA-PK; ATM; Integration

1. Introduction

Integration into the host DNA is an essential step in retroviral replication [1]. The integration of retroviral DNA is usually mediated by the viral protein integrase [2,3]. However, recent in vitro studies suggest that several host proteins also participate in the reaction. Daniel et al. [4] have reported that the integrase-mediated joining of retroviral and host DNA is recognized as damage by the host cells, and that DNA repair proteins, such as DNA-dependent protein kinase (DNA-PK), may be required to facilitate stable integration. The catalytic subunit of DNA-PK, DNA-PKcs, is a member of a family of large, presumably multifunctional, phosphatidylinositol 3-kinase (PI-3K)-related protein kinases [5,6]. DNA-PKcs is a component of the cellular, non-homologous end-joining (NHEJ) pathway and is known to be required for the repair of double-strand breaks induced by ionizing radiation and certain DNA-damaging drugs and for V(D)J recombination during the generation of immunoglobulin-producing cells [7]. The initial events in retroviral integration would be detected as DNA damage by the host cell and DNA-PK-mediated repair may be required for the completion of the integration process. Thus, DNA-PK-deficient murine *scid* cells infected with retroviruses showed a substantial reduction in retroviral DNA integration as compared with control cells because

* Corresponding author. Tel.: +81 3 5803 5399; fax: +81 3 5803 0123.
E-mail address: masa.pth2@med.tmd.ac.jp (M. Kitagawa).

0145-2126/$ – see front matter © 2005 Elsevier Ltd. All rights reserved.
doi:10.1016/j.leukres.2005.01.016

the abortive integration of retroviruses induced apoptosis [8]. However, other experiments using HIV-1-derived retroviral vectors and cultured *scid* cells revealed that DNA-PK is not required for efficient retroviral integration [9]. Thus, the roles of DNA-PK in the retroviral integration are still unclear.

The *ataxia telangiectasia mutated* (*ATM*) gene and the *ATM* and *Rad3*-related (*ATR*) gene, which also encode members of the PI-3K-related protein kinase family, play important roles in inducing cell cycle arrest in response to DNA damage and partially contribute to DNA repair. Using wortmannin (an irreversible inhibitor of PI-3K-related protein kinases including DNA-PK and ATM kinases) and a DNA-PK-deficient murine *scid* cell system, Daniel et al. [8] have shown that in the absence of DNA repair protein of the NHEJ pathway, ATM is required to allow stable retroviral integration and to avoid integrase-mediated cell killing. However, recent in vitro experiments using caffeine (an efficient inhibitor of ATM and ATR) and an ATM-deficient cell system demonstrated that ATR kinase activity was required for successful completion of the integration [10]. Thus, the identity and mechanism of action of proteins responsible for repair of the viral–host DNA in the retroviral integration process have differed among the experimental systems employed.

To clarify the overall contribution of PI-3K-related protein kinases to the retroviral integration process and their significance for retrovirus-induced pathogenesis, it is important to trace the overall process of retroviral infection in the in vivo system using PI-3K-related protein kinase-deficient hosts. Thus, in the present study, Friend leukemia virus (FLV) was introduced into DNA-PK-deficient *scid* mice and *ATM* knockout (−/−) mice with the C3H background although regrettably, the knockout of *ATR* is embryonic lethal [11]. The FLV-induced leukemogenicity in these in vivo systems was determined and retroviral infection-related events in these PI-3K-related protein kinase-deficient mice were analyzed.

2. Materials and methods

2.1. Mice

The 8–10-week-old male C3H/He (C3H) mice were bred from our colony at the Animal Production Facility of the National Institute of Radiological Sciences in Chiba. The *scid* mice and *ATM* knockout (−/−) mice with the C3H background were also bred from our colony. Methods for the generation of knockout constructs and *ATM* −/− mice were described elsewhere [12]. The *scid* and *ATM* −/− mice with the C3H background were generated by crossing CB.17 *scid* and 129/Sv *ATM* −/− mice [13] with the C3H strain, respectively, followed by backcrossing through more than 20 generations. All mice were maintained within a barrier-sustained specific-pathogen-free (SPF) facility. All animals were reared and treated in accordance with the guidelines governing the care and use of laboratory animals at the National Institute of Radiological Sciences (approval numbers 1997-4 and 1997-17) and also the guidelines established by the Animal Experiment Committee of the Tokyo Medical and Dental University.

2.2. Viral infection and determination of leukemogenesis

An NB-tropic Friend leukemia virus complex, originally provided by Dr. C. Friend, was prepared as described earlier [14] and injected i.p. into mice at a highly leukemogenic dose of 10^4 PFU/mouse [15]. The development of leukemia was assessed using the hematocrit (Ht) value (%) and the nucleated cell count (NCC) of peripheral blood from the tail vein ($\times 10^3$/mm^3) after inoculation with FLV. One, 2, 4 and 8 weeks after the inoculation, spleen cells were collected from experimental groups of mice, stained with phycoerythrin (PE)-conjugated monoclonal anti-erythroid cells (TER119, Pharmingen, San Diego, CA, USA), and analyzed on a FACScan (Becton Dickinson Immunocytometry Systems, Mountain View, CA, USA). The TER119-positive cell parameter was calculated [16].

2.3. Southern blot hybridization

To detect the integration of proviral DNA into spleen cells from the FLV-infected mice, Southern blot hybridization was performed for FLV-specific sequences of cellular DNA [17]. Chromosomal DNA was extracted from the spleen by the phenol extraction method [18] with modifications. The DNA (10 μg) digested with restriction enzymes was fractioned by electrophoresis through 0.7% agarose gel, transferred to a Magna nylon membrane (Micron Separations Inc., Westboro, MA, USA), and hybridized to a ^{32}P-labeled *env* probe derived from a 0.8-kb *Bam*HI–*Bam*HI fragment of the Friend MuLV *env* region [19]. Southern hybridization and washing were performed according to the manufacturer's instructions (Micron Separations Inc.). Briefly, hybridization was carried out at 65 °C for 16 h in 5× SSPE, 5× Denhardt's solution, 0.5% SDS and 10 μg/ml of heat denatured salmon sperm DNA. Washing was carried out at room temperature for 10 min in 2× SSC, at 65 °C for 60 min in 2× SSC and 0.5% SDS, and then at room temperature for 10 min in 0.1× SSC. Hybridization and washing were done in rotation in a hybridization oven. Hybridization signals were detected by exposing the imaging plate of a Bio Imaging Analyzer (Fuji Bas 2000, Tokyo, Japan). Because *Hin*dIII cut the Friend MuLV sequences at two sites outside of the probe-binding portion, randomly integrated viral DNA would be detected as smears. In contrast, *Bam*HI digestion cut both ends of the probe-binding portion because the probe was designed from a *Bam*HI–*Bam*HI fragment of Friend MuLV. Therefore, *Bam*HI digestion would demonstrate integrated viral DNA.

2.4. Direct PCR for detecting specific integration of FLV at the Spi-1 or Fli-1 site

To determine the precise location and transcriptional orientation of the proviruses, we directly amplified junc-

tion fragments of proviral and host DNA using proviral primers and flanking host DNA primers. These primers were synthesized by a commercial laboratory (Invitrogen Corp., Carlsbad, CA, USA). The following pairs of primers were used: a primer from the LTR of F-MuLV, P3, *F-MuLV-P3*: GTCGCCCGGGTACCCGTATTC, and a primer from the sequence of the F-MuLV integration site of *Fli-1*, *Fli-1-Pu*: CGCTGAAGGGAAGAGCAAGAG [26], and in the same way, that of *SFFF-P3*: CACTAGAATACGAGCCACGATAAAT, and that of the SFFV integration site, *Spi-1*, *Spi-1-Pu*: CTTTCACTTGTGTAGTTGAAGATGG. High molecular weight DNAs (150 ng) were subjected to 35 cycles of PCR in a final volume of 50 μl, containing 0.2 mM of each dNTP, 1 mM $MgSO_4$, 1.0 unit of KOD-Plus-DNA polymerase (Toyobo, Osaka, Japan) and 1× PCR buffer for KOD-Plus-DNA polymerase, and 0.3 μM of each primer. PCR was performed for 35 cycles of 1 min at 94 °C, 30 s at 60 °C and 3 min at 68 °C. Aliquots of 10 μl were analyzed by electrophoresis in 1.0 or 1.5% agarose gels and visualized using ethidium bromide fluorescence. λ/*Hin*dIII–*Eco*RI-cut DNA or *φXHae*III-cut DNA was run in parallel as a molecular weight marker.

2.5. Reverse transcription (RT)-polymerase chain reaction (PCR) for Spi-1 or Fli-1 expression

To determine the activation of the *Spi-1* and *Fli-1* genes which is essential for the transformation of erythroid cells during the progression of FLV-induced disease [20], RT-PCR was performed in each experimental group. The RNA was extracted from the spleen and bone marrow using an RNeasy Mini Kit (Qiagen, Valencia, CA, USA) according to the manufacturer's directions. Tissue RNA (100 ng) was used as a template for the amplification reactions. Complementary (c) DNA was synthesized using Rous-associated virus reverse transcriptase (Takara Biomedicals, Kyoto, Japan). The PCR was performed as described elsewhere [21]. Oligonucleotides as specific primers for *Spi-1* and *Fli-1* were synthesized by a commercial laboratory (Life Technologies Oriental, Tokyo, Japan). As a control reaction, β-actin was also included in each run. The sequences of primers were as follows: *Spi-1*: 5′ PCR primer ATGGAAGGGTTTTCCCTCACCGCC, 3′ PCR primer CTGCACGCTCTGCAGCTCTGTGAA; *Fli-1*: 5′ PCR primer CCAGAACATGGATGGCAAGGA, 3′ PCR primer CCCAGGATCTGATAAGGATCTGGC; β-actin: 5′ PCR primer TGGAATCCTGTGGCATCCATGA, 3′ PCR primer ATCTTCATGGTGCTAGGAGCCAG. The expected sizes of the PCR products were 216 bp for *Spi-1*, 324 bp for *Fli-1* and 175 bp for β-actin. *φX174/Hae*III-cut DNA was run in parallel as a molecular weight marker.

2.6. Bone marrow transplantation (BMT)

To determine whether hematopoietic cells of the *scid* mice were actually refractory to FLV-induced leukemia even under conditions of normal NK-cell activity, a BMT model to rescue the FLV-infected wild type C3H host was generated. The wild type C3H mice that had a normal immune function, in other words, that did not have elevated NK-cell activity, were inoculated with FLV. One week later when FLV-induced splenomegaly was evident, mice were lethally irradiated (9.5 Gy) and transplanted with 10^6 of bone marrow cells from C3H *scid* mice. As control experiments, FLV-free C3H mice transplanted with the C3H *scid* bone marrow cells and FLV-inoculated C3H mice transplanted with the wild type C3H bone marrow cells were also generated.

2.7. Detection of apoptosis

Fresh spleen tissue was mounted in an OCT compound (Sakura, Tokyo, Japan), frozen with liquid nitrogen and cut to make 8–10 μm thick frozen sections. To identify apoptotic cells on frozen tissue sections by terminal deoxytransferase (TdT)-mediated dUTP nick end labeling (TUNEL), an in situ cell death detection kit, fluorescein (Boeringer Mannheim, Mannheim, Germany) was used as described previously [22]. Briefly, frozen sections were fixed with a 4% paraformaldehyde solution for 20 min, washed with phosphate-buffered saline (PBS), incubated in 0.1% sodium citrate–0.1% Triton X-100 for 2 min, washed with PBS and then incubated with FITC-labeled dUTP and TdT at 37 °C for 60 min. Sections were then observed under a fluorescent microscope and the TUNEL-positive cell ratio was determined by dividing the number of positively stained cells by the total cell number (counting more than 1000 cells).

2.8. Western blot analysis for gp70 and p53 protein

Spleen cells from each group of mice were suspended in Iscove's modified Dulbecco's medium (IMDM, Sigma, St. Louis, CA, USA) containing 10% fetal bovine serum, at a concentration of 6×10^6 cells/tube and pelleted. Cell lysates were prepared by incubating the pellets on ice for 15 min in 1 ml of a lysis buffer containing 10 mM Tris–HCl (pH 7.5), 5 mM EDTA, 1% Nonidet P-40, 0.02% NaN_3, 1 mM phenylmethyl sulfonyl fluoride (PMSF), 0.1% aprotinin 100 μM leupeptin, and 100 μM tosyl-L-phenylalanyl chloromethyl ketone (TPCK) (Sigma). Supernatants were separated from debris by centrifugation at 12,000 rpm (9000 × *g*) for 5 min at 4 °C. Protein concentrations were determined using a Bio-Rad protein assay kit (Bio-Rad Laboratories, Hercules, CA, USA). The whole cell lysate (50 μg) was subjected to 8, 10 or 12.5% SDS-PAGE. Gels were transferred electrophoretically to nitrocellulose membranes (Schleicher and Schull, Dassel, Germany). The membranes were blocked in 10% skim milk in PBS, incubated with a goat polyclonal anti-gp70 (Quality Biotech, Camden, NJ, USA) or a mouse monoclonal antibody to P53 protein (Pab 240, Santa Cruz Biotechnology, Santa Cruz, CA, USA), and after being washed were incubated with a horseradish peroxidase-conjugated anti-

Table 1
Hematocrit (Ht) value of the peripheral blood from the wild type, *scid* and *ATM* −/− mice after inoculation with FLV

Mice	Time after inoculation with FLV				
	Control	1 Week	2 Weeks	4 Weeks	8 Weeks
C3H wild	51 ± 1.0	48 ± 1.0	38 ± 2.0	31 ± 4.3	21 ± 5.5[a]
C3H *scid*	46 ± 0.7	43 ± 1.5	41 ± 0.3	36 ± 3.8	38 ± 1.6[a,b]
C3H *ATM* −/−	45 ± 2.6	48 ± 5.0	42 ± 1.5	30 ± 1.7	23 ± 6.4[b]

Values indicate the mean ± S.D. of the Ht value (%) of peripheral blood in three to five mice from each experimental group. Note the gradual decrease in the Ht value of wild type and *ATM* −/− mice, 2 and 4 weeks after FLV inoculation, in contrast to the slight increase or normal level in the FLV-inoculated *scid* mice.
[a] Differences were significant between the C3H control and *scid* mice at 8 weeks after FLV inoculation using Student's *t*-test ($p < 0.01$).
[b] Differences were significant between the *scid* and *ATM* −/− mice at 8 weeks after FLV inoculation using Student's *t*-test ($p < 0.01$).

goat or anti-mouse IgG antibody (Dakopatts, Glostrup, Denmark). To confirm the equivalent loading of protein in each lane, membranes were blocked, incubated in polyclonal rabbit anti-actin antisera (Sigma), and after washing, incubated in horseradish peroxidase-conjugated anti-rabbit Ig antibody (Dakopatts). Bands in the washed membrane were detected with an enhanced chemiluminescence (ECL) system (Amersham Life Science, Buckinghamshire, UK) as described previously [22].

2.9. Densitometric analysis

The densities of bands were measured by densitometric analysis with an ImageQuant scanning imager (Molecular Dynamics, Sunnyvale, CA, USA). The relative intensities of the bends were calculated by comparing the density of the sample with that of the control.

3. Results

3.1. FLV-induced leukemogenesis in the scid and ATM −/− mice

First, to determine the leukemogenicity of FLV in DNA-PK-deficient *scid* mice and *ATM* −/− mice, parameters including the hematocrit (Ht) value, nucleated cell count (NCC) of peripheral blood, spleen weight and TER119-positive cell ratio of the spleen were determined after inoculation with a leukemogenic dose of FLV. As shown in Table 1, Ht values declined remarkably after FLV inoculation in the wild type and *ATM* −/− C3H mice. In contrast, the *scid* mice showed only a slight decrease in the Ht value. Regarding the NCC, spleen weight and TER119-positive cell ratio, FLV-inoculated wild type and *ATM* −/− mice showed a gradual but significant increase after the inoculation with FLV, while *scid* mice showed very slow or no remarkable change (Fig. 1). As shown in Fig. 2, all the FLV-inoculated wild type mice died from leukemia within 19 weeks and the *ATM* −/− mice within 15 weeks, while only 20% of the FLV-inoculated *scid* mice died from leukemia; the majority of mice lived for more than 24 weeks with no evidence of splenomegaly. The *ATM* −/− mice seemed more susceptible to FLV-induced leukemia than the wild type mice probably due to their immunodeficient nature [23,24]. These findings indicated that FLV inoculation induced leukemia in the wild type and *ATM* −/− mice, whereas, the *scid* mice were significantly refractory to FLV-induced leukemogenesis.

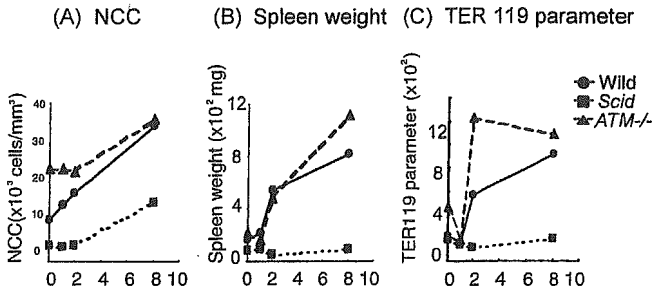

Fig. 1. FLV-induced leukemogenicity in mice with the C3H background. Lines indicate the wild type (●), *scid* (■) and *ATM* −/− mice with the C3H background (▲). Parameters for the leukemogenicity are: (A) nucleated cell count of peripheral blood ($\times 10^3$/mm^3); (B) spleen weight ($\times 10^2$ mg); (C) TER119-positive cell parameter of the spleen (spleen weight (mg) × TER119-positive cell ratio (%)/body weight (g)). Note that FLV-inoculated wild type mice and *ATM* −/− mice exhibited an increase in these parameters indicating the induction of leukemia, 4 and 8 weeks after inoculation with FLV, while *scid* mice revealed only a slight increase in each parameter.

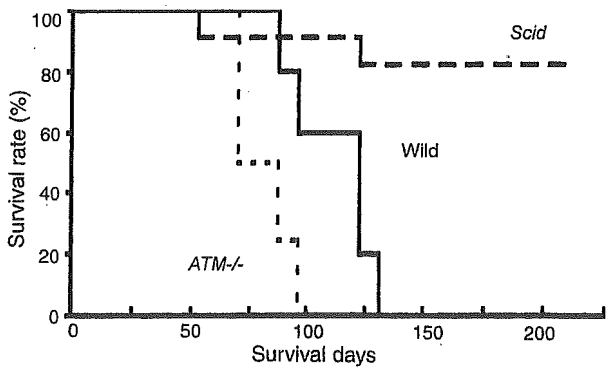

Fig. 2. Survival curves of the mice with the C3H background after inoculation with FLV. Lines indicate the wild type (solid line, $n = 10$), *scid* (broken line, $n = 13$) and *ATM* −/− (dotted line, $n = 8$) mice with the C3H background. Note the significantly longer survival of the FLV-inoculated *scid* mice compared with the FLV-inoculated wild type or *ATM* −/− mice ($p < 0.01$ and $p < 0.001$ using the Mantel–Cox test, respectively). In addition, the survival of *ATM* −/− mice was significantly shorter than that of wild type mice ($p < 0.05$).

3.2. Integration of FLV in spleen cells from the FLV-infected scid and ATM −/− mice

To investigate the actual integration of FLV into the host DNA of the *scid* and *ATM* −/− mice, Southern blot hybridization was performed to detect FLV-specific sequences in the host genome. As shown in Fig. 3A, randomly integrated FLV sequences were detected by *Hin*dIII digestion as smears, and as shown in Fig. 3B, *Bam*HI digestion demonstrated the overall integrated sequences as clear bands in spleens from the wild type and *ATM* −/− mice, 1 and 4 weeks after inoculation with FLV. Integrated signals were also clearly detected in samples from the *scid* mice, although the densities of the bands were slightly weaker. Analysis using densitometry revealed that the intensity of integration signals in *scid* mice was 2–3-fold less than those of wild mice and that the intensities in *ATM* −/− mice was almost two thirds of those of wild mice. These results suggested that the random integration of FLV did occur in the wild type and *ATM* −/− mice and also in the *scid* mice as well, although the integration efficiency seemed lower especially in *scid* mice.

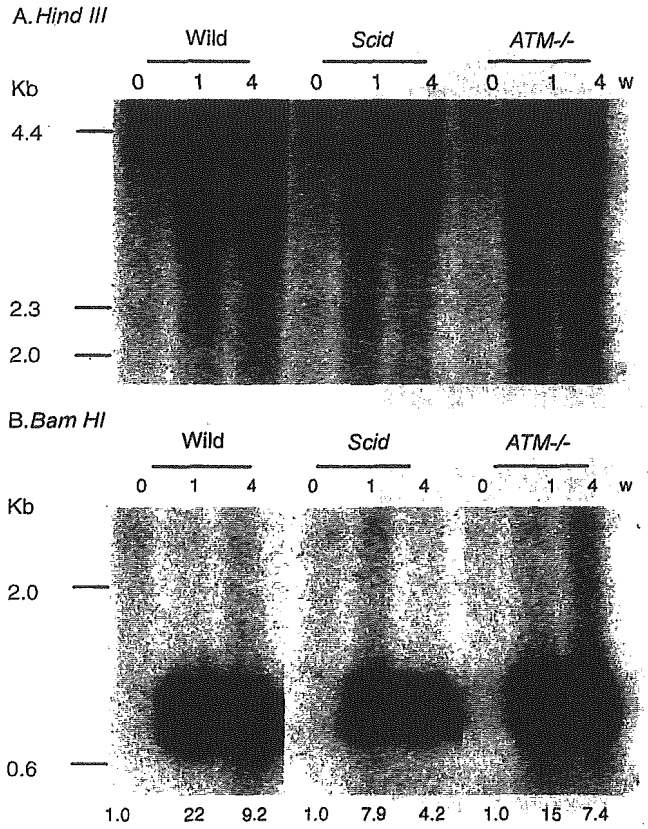

Fig. 3. Southern blot hybridization analysis for FLV-specific sequences in host DNA of the wild type, *scid* and *ATM* −/− mice after inoculation with FLV. Genomic DNA (10 μg) of high molecular weight prepared from each experimental group of mice was digested with *Hin*dIII (A) and *Bam*HI (B). Each sample was hybridized with a ^{32}P-labeled Friend MuLV-derived DNA probe. *Hin*dIII digestion was expected to detect randomly integrated F-MuLV DNA as smears and free viral cDNA as bands. In contrast, *Bam*HI digestion would reveal integrated or free DNA as distinct bands. As we could detect smear signals but not band signals in *Hin*dIII digestion experiments, free viral cDNA would be ignorable probably because we prepared the samples by a high molecular weight DNA extraction method. Note that the integrated proviral sequences of F-MuLV were prominent in the wild type and *ATM* −/− mice, 1 and 4 weeks after inoculation with FLV. The *scid* mice also demonstrated significant integration although the density of bands appeared slightly weaker. The relative intensities of bands were measured by densitometry (wild mouse sample before inoculation with FLV as the control, 1.0) and indicated under the photos of gels.

3.3. Expression of gp70 protein in spleen cells of the wild type, scid and ATM −/− mice

To confirm whether the integrated viral genes were actually expressed, the viral envelope protein gp70, was examined by Western blotting after inoculation of the wild type and *scid* mice. As shown in Fig. 4, gp70 was abundantly expressed in the spleen cells of wild type mice, 1, 4 and 8 weeks after the inoculation with FLV. In the *scid* mice also, spleen cells exhibited significant signals at 1, 4 and 8 weeks, although the expression of gp70-associated protein was observed as early as 1 and 3 days in *scid* mice. However, the overall expression of gp70 was slightly lower in the *scid* mice than the wild type mice. These findings were consistent with the data shown in Fig. 3A and B indicating the levels of FLV integration into spleen cells of the wild type and *scid* mice.

3.4. Integration of FLV at Spi-1 and Fli-1 sites and the expression of Spi-1 and Fli-1 in spleen cells of the wild type, scid and ATM −/− mice

Spi-1 and *Fli-1* are transcription factors expressed in the majority of FLV-induced leukemia cells [25,26]. Integration of the spleen focus forming virus (SFFV) occurs at the *Spi-1* site and that of the Friend murine leukemia virus (MuLV) adjacent to the *Fli-1* site. The integrated LTR of the virus promotes the expression of these transcription factors causing leukemogenesis. To detect the specific integration of viral sequences at these sites, direct PCR analysis was performed using primer sets amplifying junction fragments of the integrated viral sequences and the host transcription factor sequences. As shown in Fig. 5A, dilution experiments were performed using PCR products for the *Spi-1* site detected 1 week after inoculation with FLV and those for the *Fli-1* site by week 8 in spleen cells of the wild type mice. Both signals were evident in 5× and 1× (no dilution) samples. Then, the PCR was performed for samples from 0, 1 and 8 weeks after inoculation with FLV in wild type, *scid* and *ATM* −/− mice. As shown in Fig. 5B, PCR products for the *Spi-1* site were detected 1 week after inoculation with FLV and those for the *Fli-1* site by week 8 in spleen cells of the wild type and *ATM* −/− mice, These findings indicate that the monoclonal expansion of leukemic cells occurs with integration of SFFV at the *Spi-1* site at an early stage and later with the integration of F-MuLV at the *Fli-1* site. In contrast, spleen cells from the *scid* mice exhibited a very weak signal for *Spi-1* site integration and the undetectable level of *Fli-1* site integration signal

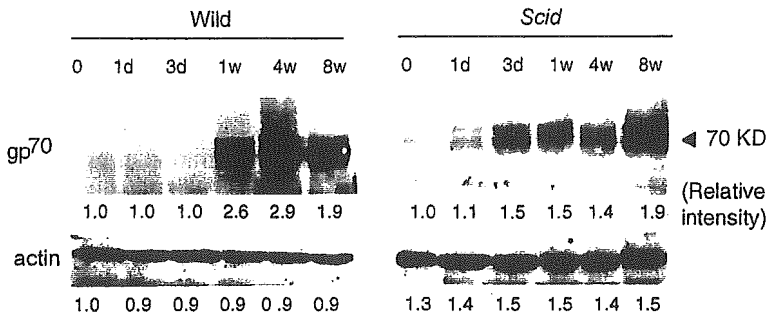

Fig. 4. Expression of gp70 in the C3H wild type and *scid* mice determined by Western blotting. The relative intensities of bands were measured by densitometry (0 day, wild type as the control, 1.0) and indicated under the photos of gels. Note that the expression of gp70 was prominent in the wild type mice, 1, 4 and 8 weeks after inoculation with FLV. The *scid* mice expressed gp70 from the earlier period after FLV inoculation (1 and 3 days) probably originated from the immunodeficient nature of these mice. In 1, 4 and 8 weeks, *scid* mice demonstrated significant expression although the density of bands in 1 and 4 weeks appeared slightly weaker than the wild type.

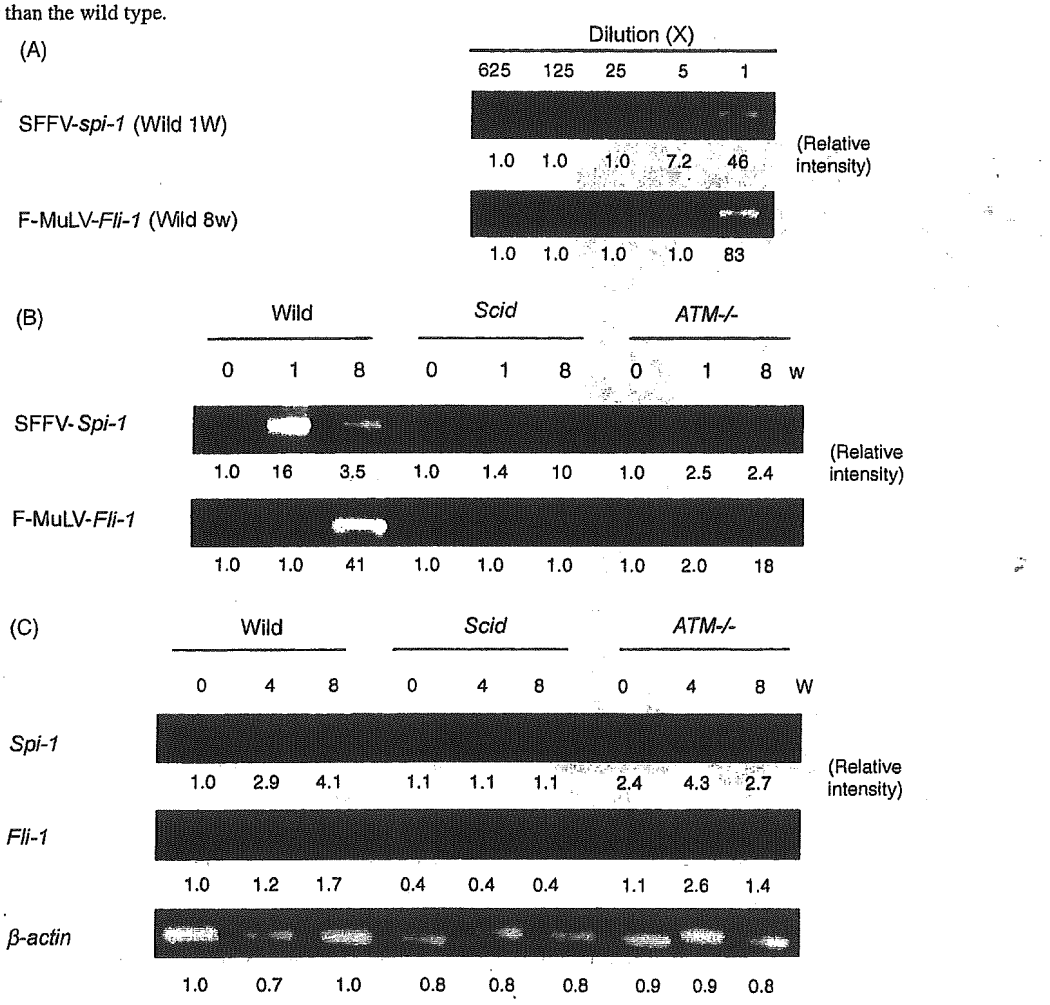

Fig. 5. Specific integration of FLV and expression of the transcription factors. Direct PCR analysis for the specific integration of FLV at the *Spi-1* or *Fli-1* site (A) and RT-PCR analysis for the mRNA expression of *Spi-1* and *Fli-1* (B) in the spleen of mice with the C3H background. DNA or RNA samples were prepared from the spleen of wild type, *scid* and *ATM* −/− mice, before and 1 and 8 weeks after inoculation with FLV. (A) DNA samples from wild type mice were prepared 1 and 8 weeks after inoculation with FLV and diluted to 5×, 25×, 125× and 625×. Direct PCR was performed for SFFV-*Spi-1* in samples from week 1 with each dilution or F-MuLV-*Fli-1* in samples from week 8. The relative intensities of bands were measured by densitometry (625× sample as the control, 1.0) and indicated under the photos of gels. Note that both signals were evident in samples 5× and 1×. (B) Direct PCR exhibited integration of SFFV at the *Spi-1* site (1 week after FLV inoculation) and F-MuLV at the *Fli-1* site (4 weeks after FLV inoculation) in spleen cells from the wild type and *ATM* −/− mice. In contrast, very weak signal was observed in spleen cells from the *scid* mice for *Spi-1* site integration and the signal was not detectable for the *Fli-1* site integration. The relative intensities of bands were measured by densitometry (0 day, wild type as the control, 1.0) and indicated under the photos of gels. (C) A RT-PCR technique revealed overexpression of mRNA for *Spi-1* and *Fli-1* in the FLV-infected wild type and *ATM* −/− samples, 4 and 8 weeks after FLV inoculation. However, up-regulation was not detectable in samples from FLV-inoculated *scid* mice. The relative intensities of bands were measured by densitometry (0 day, wild type as the control, 1.0) and indicated under the photos of gels.